Journal of Nanobiotechnology

RESEARCH

Open Access

Rapid diagnostic imaging and targeted immunotoxin delivery in aggressive prostate cancer using CEACAM5-specific nanobodies

Zhaoming Xiao[1,2†], Jingbo Ma[3†], Jinpeng Cen[2†], Tao Xie[4†], Liuhai Zheng[3], Guangwei Shi[3,5], Zhifen Li[6], Yang Li[3], Chengming Qu[3], Yuanqiao He[7,8], Chong Wang[4], Jun Xiao[2], Haibo Jiang[9], Zhijie Li[3*], Jigang Wang[3,10,11,12,13,14*] and Shan-Chao Zhao[1,2,15*]

Abstract

Aggressive variant prostate cancer (AVPC) originates from metastatic prostate cancer (mPCa) following androgen receptor-targeted therapies, leading to diverse pathological subtypes, notably castration-resistant prostate cancer (CRPC). Carcinoembryonic antigen-related cell adhesion molecule 5 (CEACAM5), is consistently expressed across AVPC phenotypes, including neuroendocrine prostate carcinoma (NEPC) and double-negative prostate carcinoma (DNPC), which are significant subtypes of CRPC, making it a promising therapeutic target. In this study, A high-affinity nanobody, B12, specific to CEACAM5, was discovered through phage library screening. B12 exhibited robust binding capabilities, enhanced tumor accumulation, and effective tissue penetration, facilitating rapid in vivo imaging of AVPC. The conjugation of B12 with PE38 to create the immunotoxin B12-PE38 showed significant anti-tumor activity in AVPC xenograft models, including one that mimics bone metastasis. When B12-PE38 was combined with docetaxel, it elicited enhanced tumor inhibitory effects, effectively inhibiting tumor progression. This study underscores CEACAM5 as a target for precise imaging and targeted therapy in AVPC, introducing novel diagnostic and therapeutic strategies for a disease that currently faces a dearth of effective treatment options due to the scarcity of well-defined targets.

Keywords Aggressive variant prostate cancer, Phenotype transformation, CEACAM5, Nanobodies, Rapid imaging, Immunotoxin

†Zhaoming Xiao, Jingbo Ma, Jinpeng Cen, and Tao Xie have contributed equally to this work and share the first authorship.

*Correspondence:
Zhijie Li
li.zhijie@szhospital.com
Jigang Wang
jgwang@icmm.ac.cn
Shan-Chao Zhao
lulululu@smu.edu.cn
Full list of author information is available at the end of the article

Graphical Abstract

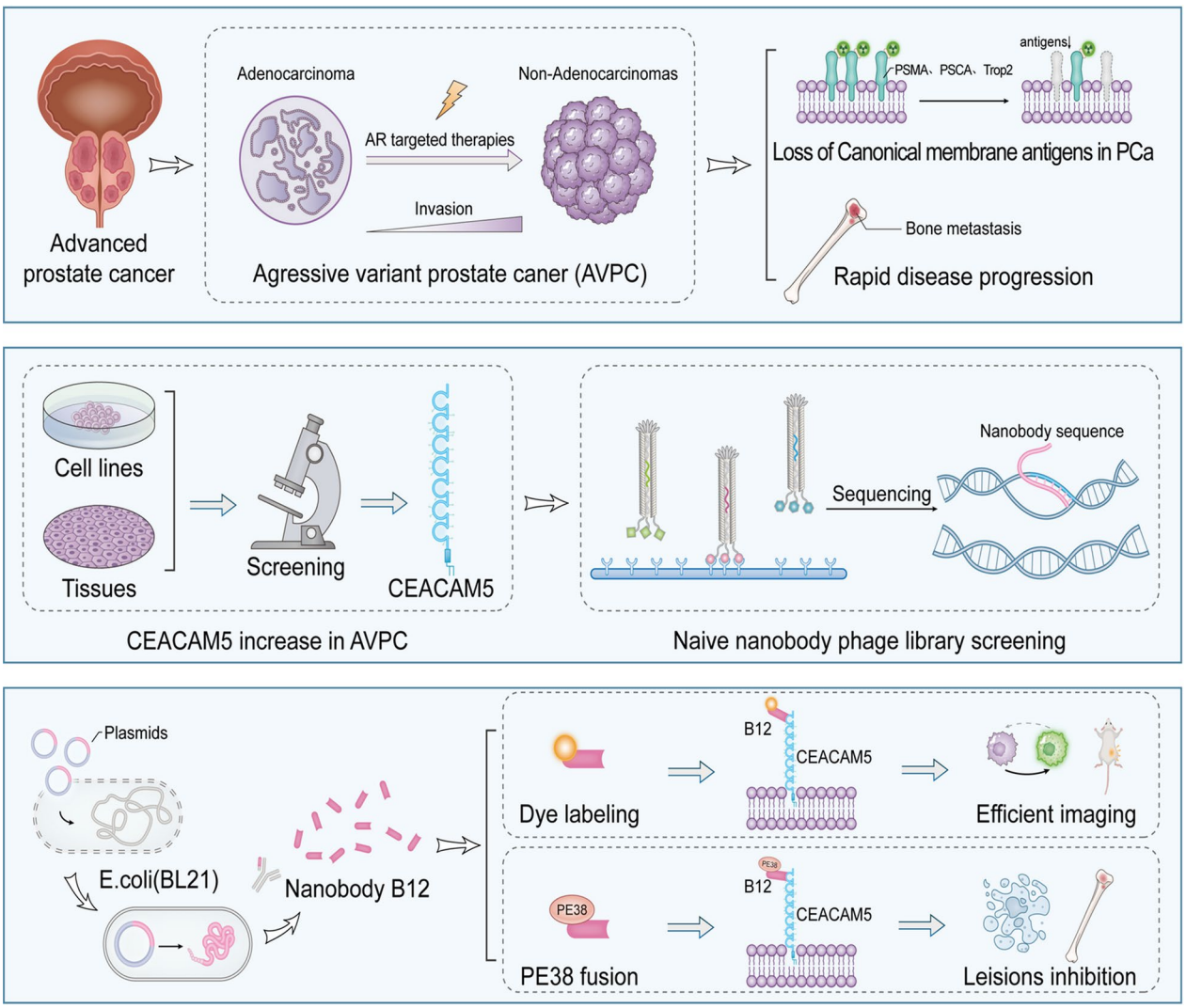

Introduction

Androgen deprivation therapy (ADT) enhanced with the complete blockade of endogenous androgen synthesis (abiraterone) or targeting inhibition of androgen receptor (AR) transduction (enzalutamide) has significantly benefited patients with advanced prostate adenocarcinoma (PRAD) and prolonged overall survival [1–4]. However, most patients receiving androgen-targeted therapies inevitably progress to CRPC or metastatic CRPC which is the main death cause for prostate cancer.[5–8]. Nevertheless, up to 10–20% of CRPC cases eventually evolve into another progressive subtype, namely NEPC, which is characterized by upregulation of neuroendocrine markers such as synaptophysin (SYN/SYP) and chromogranin A (CGA) [9]. Recent studies also disclosed another subtype for CRPC, known as a double negative phenotype (DNPC, AR- and neuroendocrine-negative) [10]. Both of them result from the selective pressure of androgen-targeted therapies and are lethal aggressive variant prostate cancers (AVPC), leading to an adverse prognosis, and requiring early disease detection and new treatment strategies [11, 12]. Two essential surface targets prostate stem cell antigen (PSCA) and prostate membrane antigen (PSMA) have been explored to develop various diagnostic and therapeutic strategies for advanced metastatic prostate cancers including CRPC. Targeting PSMA with 177Lu-PSMA-617 has been approved for metastatic CRPC. Unfortunately, up to 40% CRPC show low or

absent expression of PSMA, and both of biomarkers are almost undetectable in NEPC and DNPC [13–15]. Therefore, it is still challenging to timely and precisely diagnose and treat AVPC due to the lack of specific tumor cell surface markers to develop targeting strategies [16].

The membrane antigen carcinoembryonic antigen-related cell adhesion molecule 5 (CEACAM5), also known as CEA or CD66e, pathologically and abnormally expressed during carcinogenesis of respiratory and digestive organs, has long been recognized as a cancer diagnosis biomarker and therapeutic target in multiple cancers. A diversity of strategies directing CEACAM5 have been developed and tested in preclinical and clinical settings for cancer imaging and therapy, including but not limited to immuno-PET, targeted fluorescence imaging, imaging-guided surgery, tumor vaccines, bispecific immune cell engagers, chimeric antigen receptor T/NK-cell therapies (CAR-T/NK), and antibody–drug conjugates (ADCs) [15, 17–23]. Intriguingly, CEACAM5 was also found upregulation in NEPC [14, 24]. Further studies reveal that compared with other prostate cancer antigens such as trophoblast cell surface antigen 2 (Trop2), PMAS, PSCA and delta-like ligand 3 (DLL3), CEACAM5 is more specifically expressed and elevated in NEPC and DNPC across four clinically relevant subtypes of prostate cancers including AR-positive PC (ARPC), NEPC, DNPC and amphicine PC (AMPC), implicating that CEACAM5 could be potentially exploited as an imaging and therapeutic target for AVPC. Since various modalities targeting CEACAM5 have been developed and evaluated for other epithelial malignancies preclinically and clinically, it is more feasible for these modalities to be rapidly tested in CEACAM5$^+$ NEPC and DNPC when compared with new antigens identified. Labetuzumab govitecan, an well-characterized ADC against CEACAM5 has been evaluated in a preclinical CEACAM5$^+$ PCa model, demonstrating the promising tumor inhibitory efficacy [15]. Similarly, CAR-T cells targeting CEACAM5 could also slow down the progression in a CEACAM5$^+$ PCa model [23]. Both of therapeutic strategies demonstrate the great potential of CEACAM5 as a diagnostic and therapeutic biomarker for the formidable AVPC, in particular NEPC and DNPC.

Currently, full-length antibodies are most commonly used for the development of CEACAM5-targeted therapeutic and diagnostic modalities, owing to their high affinity and the advanced technologies available for antibody production and optimization. However, the relatively large molecular weight around 150kD restricts their tumor penetration and bio-distribution, and the long half-life of antibodies makes them unfeasible for rapid tumor imaging [15, 22, 25, 26]. Engineered from variable heavy region of heavy chain-only antibody (VHH) originated from camelids, nanobodies demonstrate several superior advantages over full-length antibodies on bio-distribution and tissue penetration due to its small size around 15kD [27, 28]. Moreover, nanobody can be easily and efficiently prepared through prokaryotic expression system [27, 28]. In this study, a CEACAM5 targeted nanobody B12 was identified through three rounds biopanning from a naïve phage nanobody library, which not only exhibited a strong affinity against CEACAM5 antigen in vitro, but also facilitated rapid in vivo imaging of AVPC, especially in tumor subtype DNPC derived PC3 xenograft with moderate CEACAM5 expression. Moreover, this nanobody fused with a bacteria toxin PE38 could efficiently deliver toxin to CEACAM5$^+$ PC3 cell-derived xenografts (CDX) and CEACAM5$^+$ patient-derived xenografts (PDX), markedly suppress the tumor progress, and improve antitumor effect when combined with docetaxel. More importantly, the B12-PE38 immunotoxin effectively inhibited the intra-tibial lesions induced by PC3 cells.

Methods and materials

Cell lines and cultures

In this study, a variety of prostate, gastric, and colorectal cancer cells were used. The cell lines (LNCAP, C4-2, 22RV1, PC3, DU145, VCAP, NCI-H660, HT29, MKN45) were obtained from Yanshun Biotechnology Company (Shenzhen, China), Meisen CTCC Company (Zhejiang, China), the American Type Culture Collection (ATCC, Manassas, VA), Cell Bank of Chinese Academy of Sciences (Shanghai, China), and Fuheng Biology (Shanghai, China). LNCAP, C4-2, 22RV1, and HT29 cells were cultured in RPMI 1640 medium (Gibco, USA) supplemented with 10% fetal bovine serum (FBS), 2 mM L-glutamine, and 1% penicillin/streptomycin. DU145, VCAP, and MKN45 cells were maintained in high-glucose Dulbecco's Modified Eagle's Medium (DMEM) supplemented with 10% FBS, 2 mM L-glutamine, and 1% penicillin/streptomycin. The PC3 cell line was cultured in Ham's F-12 K medium (Procell) with 10% FBS and 1% penicillin/streptomycin. The NCI-H660 cell line was cultured in RPMI 1640 medium (Gibco, USA) with 10 nM beta-estradiol, 10 nM hydrocortisone, 1×ITS (Insulin-Transferrin-Selenium), 5%FBS, and 1% penicillin/streptomycin. All cell lines were incubated at 37 °C in a humidified atmosphere containing 5% CO2.

Sample sources

In the study, the samples included: 4 clinical samples of NEPC collected from The Fifth Affiliated Hospital, Southern Medical University. Additionally, patient-derived xenograft (PDX) samples were obtained from Prof. Yuanqiao He. All patients provided informed

consent to participate in the research project. The collection and research use of patient tissues were conducted with the consent and under the supervision of the ethics committee of The Fifth Affiliated Hospital, Southern Medical University. Tissue microarrays of normal human visceral organs, benign prostatic hyperplasia, and prostatic adenocarcinoma were all from a biobank Zhongke Guanghua Company (China).

Immunohistochemistry staining

To analyze and evaluate the expression level of CEACAM5 in prostate cancer tissue, immunohistochemical staining for CEACAM5 was performed on clinical samples of NEPC, PDX samples, CDX samples, and tissue microarrays of normal human visceral organs, benign prostatic hyperplasia, and prostatic adenocarcinoma. The sections were stained with a rabbit monoclonal Anti-CEACAM-5/CD66e Antibody (11077-R327, Sinobiological Inc. China). CEACAM5 detection was carried out using a biotin-conjugated goat anti-rabbit IgG secondary antibody and an ABC kit (Vector Laboratories, USA), followed by colorimetric detection with diaminobenzidine (DAB; Vector Laboratories, USA). The images were captured using a 3DHISTECH™ scanner (Sysmex, UK). In the pathological analysis, five visual fields were selected from each pathological section to calculate the mean positive rate per sample, thereby determining the positivity presented graphically.

Flow cytometry assay

To analyze the cell surface expression of CEACAM5 protein, flow cytometry was employed. The cells were first gently washed twice with precooled PBS, followed by enzymatic digestion using 0.25% EDTA. Subsequently, the cells were fixed with 0.25% freshly prepared PFA for 5 min at room temperature (RT) and then blocked with 3% BSA. After blocking, the Alexa Fluor® 647 conjugated anti-human CEACAM5 antibody (392806, Biolegend, USA) was added to the cells at a dilution of 1:100 and incubated on ice for 1 h. Finally, the cells were washed three times with PBS before being analyzed using a Beckman Coulter flow cytometer and FlowJo software.

Phage library screening for CEACAM5-targeted nanobody

The nanobody screening was conducted as previously described [29]. Briefly, the isolation of CEACAM5-targeted targeted nanobodies was performed with a naive phage nanobody library screening (1×10^9 diversity) (KTSM-CND002, Shenzhen KangTi Life Technology Co., Ltd. China,). The Naïve nanobody phage library was established on PBMC RNA from over 100 alpacas Alpaca (Lama pacos) and three rounds of bio-panning were performed in the immune tubes coated with 40 μg CEACAM5-Fc protein (11077-H02H, Sinobiological Inc. China). This was followed by an incubation with 3% BSA-PBS solution for 1 h at RT. The nanobody phage library was then incubated in the tube for 1 h at RT. Unbound phage clones were removed by washing with PBST (PBS + 0.1% Tween20). Bound phages were eluted using a trypsin solution (0.25 mg/ml) and neutralized with AEBSF (4 mg/ml). The eluted phage clones were amplified, rescued with M13 helper phages in E. coli TG1 cells, and precipitated using PEG–NaCl (a solution of 20% PEG 800 and 2.5 M NaCl), after which they were resuspended in PBS. The phage library was collected for titration and subsequent screening rounds. One round subtractive screening with Fc fragment prior to third round selection was conducted to remove the potential Fc binders. After three rounds of biopanning, 96 phage clones were randomly selected and amplified for phage ELISA analysis.

Briefly, microtiter plates were coated with 2 μg/ml of purified CEACAM5-Fc or Fc fragment and incubated overnight at 4 °C. After blocking with a 3% BSA solution for 1 h at RT, phage clones were added and the plates were incubated for an additional hour at RT. The plates were then washed three times with PBST to remove unbound phages. Subsequently, an HRP-conjugated anti-M13 monoclonal antibody (Sino Biological, Beijing, China) was added and the plates were incubated for 1 h at RT. After another round of washing with PBST, the plates were developed with the TMB peroxidase substrate. The reaction was halted with 1 M HCl, and the absorbance was measured at 450 nm using an automated microplate reader (LabServ K3 TOUCH, Thermo Fisher Scientific, USA). Clones exhibiting an absorbance value more than threefold higher with CEACAM5-Fc compared to Fc fragment were considered positive. Based on the ELISA results, 8 positive clones were identified, and after sequencing, two unique sequences were obtained.

Protein purification

The various nanobodies were purified as described previously [29, 30]. Briefly, the recombinant plasmids pET-22B-B12 were transformed into BL21 (DE3) and then the bacterial clones were incubated at 37 °C and 200 rpm until reaching 0.6 of OD600 value, followed by induction with 1.0 mM IPTG at 30 °C and 200 rpm overnight. The cultures were pelleted with 8000 g for 15 min at 4 °C. Cell pellets were resuspended into PBS containing polymyxin B (10000unit/ml) to release B12 nanobodies from bacterium periplasm through incubation at 37 °C and 220 rpm shake for 2 h.

The lysate was spun down for 45 min at 12,000 × g, and the supernatants were loaded on a gravity column with 1 mL Ni–NTA agarose resin (Qiagen, Germany). The protein-bound resin was washed with 50 mL Wash

Buffer I (300 mM NaCl, 50 mM NaH_2PO_4, 20 mM imidazole, pH 8.0, 1 mM PMSF) and 50 mL Wash Buffer II (300 mM NaCl, 50 mM NaH_2PO_4, 40 mM imidazole, pH 8.0, 1 mM PMSF) and then eluted with 25 ml Elution Buffer (300 mM NaCl, 50 mM NaH_2PO_4, 250 mM imidazole, pH 8.0, 1 mM PMSF). Finally, the eluate was then fractionated using a Superdex-150 gel filtration column with an AKTA Pure System (GE Healthcare Life Sciences, USA) in 1×PBS. The purified protein was identified by SDS-PAGE, quickly frozen in liquid nitrogen, and stored at −80 °C until use. Control Nb, B12-PE38, Con-PE38, B12-PE38 mut and ConNb-PE38 mut were induced using the same procedures as B12 nanobody, but all these proteins were purified as cytoplasmic proteins for which cell pellets were dissolved in lysis buffer (300 mM NaCl, 50 mM NaH_2PO_4, 10 mM imidazole, pH 8.0, 1 mM PMSF) and crushed through three cycles of low-temperature, high-pressure homogenization. The subsequent protein purification procedures are the exact same as B12 nanobodies. The purified proteins were analyzed and identified by western blot with 6×His tag, HA tag or anti-VHH antibodies.

ELISA assay

To verify the binding activity of the B12 nanobody to CEACAM5, ELISA was performed using the following procedure: 5 μg/ml of human CEACAM5 (CE5-H5226, ACRO biosystems, China) was coated onto 96-well microplates and incubated at 4 °C overnight. Unbound protein was removed by washing with PBS before incubation with a 3% BSA-PBS solution for 1 h at RT. The nanobodies were diluted from 8 to 1 nM with 1×PBST and incubated in the plates at RT for 1 h. The plates were then washed three times with 1×PBST, and the nanobodies were detected using an HRP-conjugated anti-HA tag antibody (SinoBiological, China) and TMB peroxidase substrate (BioLegend, San Diego, CA, USA). The absorbance was measured at 450 nm.

SPR assay

The experiment was used to validate the direct interaction between B12 nanobody and in antigen CEACAM5 to calculate the equilibrium constants of the two proteins. CEACAM5-his protein was purchased from ACRO biosystems company (CE5-H5226). CEACAM5 was immobilized on a chip, and different concentrations of nanobody B12 were sequentially added to analyze the binding affinity. The reaction signals were recorded within 360 s, to draw kinetic curves, and calculate each corresponding parameter.

Protein labeling with IR800

IR800 dye-labeled nanobodies were used for cell ELISA and in vivo imaging. Briefly, B12 or control nanobodies were diluted to a concentration of 1 mg/mL in PBS (pH 6.5). IR800-maleimide was added and the mixture was incubated for 2 h at RT in the dark. Unconjugated dye was removed using a 10 kDa molecular weight cut-off spin desalting column (Millipore). The concentrations of the nanobodies were measured using a BCA protein assay kit (Pierce). The proteins (B12-PE38, ConNb-PE38, B12-PE38 mut and ConNb-PE38 mu) were also labeled using the same procedure.

Cell ELISA

To analyze the binding activity of B12 nanobodies to cancer cell lines expressing CEACAM5, Cell ELISA was performed as follows: Cancer cell lines (PC3, HT29) were cultured in 96-well plates at a density of 5×10^4 cells/well overnight. The cells were fixed with 4% paraformaldehyde for 10 min and then washed once with PBST, followed by incubation with a 3% BSA for 1 h at RT. The nanobodies, previously labeled with Dye IR800 as described above, were diluted from 250 to 0 nM with 1×PBST and incubated with the plates at RT for 1 h. After washing the plates three times with PBST, fluorescence intensity was measured using a 784 nm laser channel on a Sapphire Capture system (Sapphire, USA).

In vivo imaging

Once tumors had grown to approximately 500 mm^3, the PC3 tumor-bearing mice were randomly assigned to two groups (n = 3) and injected intravenously 80 μg B12-IR800 and ConNb-IR800 respectively. At various time points post-injection, fluorescence imaging was conducted using the IVIS Spectrum system (PerkinElmer, USA). Upon completion of the whole-body image, the animals were euthanized, and key organs (heart, liver, spleen, lungs, kidneys) along with the tumors were extracted for ex vivo fluorescence analysis. In vivo imaging with various proteins, including B12-PE38 mut-IR800 and ConNb-PE38 mut-IR800, was conducted following identical procedures.

In vitro internalization and uptake assay of immunotoxins

B12-PE38 was labeled with Cy5 Dye at a 2:1 ratio as previously described. For uptake assays, 1×10^5 PC3 cells were plated in poly-lysine-coated 24-well plates and exposed to varying concentrations of B12-PE38 over different durations to assess drug uptake efficiency. After washing, cells were fixed with 4% paraformaldehyde for 10 min, and fluorescence was quantified using an inverted microscope and Image J software with a

minimum of three replicates. Flow cytometry was also used to evaluate B12-PE38 uptake in PC3 cells, with cells collected, washed, fixed, and resuspended in PBS for APC channel fluorescence detection.

In vitro cell viability assay

To verify the targeted cytotoxicity of B12-PE38 on cancer cells expressing CEACAM5 protein, CCK8 (Cell Counting Kit-8) assay was conducted to determine the cytotoxicity and the half-maximal inhibitory concentration (IC50) values. PC3, MKN45, and HT29 cells were seeded into 96-well plates at a density of 5×10^3 cells per 100 μL of culture medium per well. Following overnight incubation in a humidified atmosphere at 37 °C with 5% CO2, the cells were briefly washed once with PBS. Subsequently, different concentrations (0, 15.625, 31.25, 62.5, 125, 250, 500, and 1000 nM in 100 μL of culture medium, n = 3) of the purified B12, B12-PE38, Con-PE38, or B12-PE38 mut were introduced into the respective wells. The plates were then incubated for 3 days at 37 °C in a humidified incubator. Afterward, 10 μL of CCK-8 solution (Abcam, China) was carefully added to each well, taking care to avoid bubble formation. The plates were incubated for an additional hour at 37 °C. The absorbance was measured at 450 nm using an automated microplate reader (LabServ K3 TOUCH, Thermo Fisher Scientific, USA) following a brief shaking step. Data analysis for cell viability and IC50 values was performed using GraphPad Prism software.

EDU assay

The EDU assay kit was purchased from Biosharp Company (China). A total of 1×10^5 cells were seeded in a 96-well plate and cultured overnight. The cells were then treated with complete medium containing a gradient of concentrations of B12-PE38, or with PBS as a baseline control, as well as with B12 and ConNb-PE38 as negative controls, for approximately 12 h. Following this treatment, the EDU solution was diluted in complete medium at a ratio of 1:1000 and incubated with the cells for 2 h to label DNA synthesis. After aspirating the medium and washing the cells twice with PBS, they were fixed with a 4% paraformaldehyde solution for 10 min to preserve cellular morphology. Subsequently, EDU-positive cells were detected using the protocol recommended by the kit, and the nuclei were counterstained with Hoechst 33342 to visualize cell nuclei. Finally, at least three replicates of fluorescence images were captured using an inverted microscope, and the data were analyzed to calculate the differences in cell proliferation rates.

Mouse xenograft models and treatments

All experiments on animals in the present study were done following the approved protocol by Institutional Animal Care and Use Committee (IACUC) of the Shenzhen People's hospital and were carried out in accordance with relevant institutional and national guidelines and regulations. Nude mice and NCG mice at 6–8 weeks old were purchased from Gempharmatech (Guangzhou, China) and were maintained under pathogen-free conditions in the animal center of the Shenzhen People's hospital. Mice were euthanized when showed obvious signs of discomfort or when maximal tumor size reached 2000 mm^3.

To establish the subcutaneous tumor models, 100 μl of PBS containing approximately 5×10^6 PC3 cells, 2×10^6 HT29 cells was injected into the right lower back of the mice. Tumor size was measured with vernier calipers and calculated using the following formula: (length × width × width)/2.

To determine the antitumor efficacy of B12-PE38, PC3 tumor-bearing mice were first selected for antitumor study. In brief, tumor-bearing mice were randomly divided into control group (PBS), control group (B12), low-dose group (0.4 mg/kg B12-PE38), and high-dose group (0.6 mg/kg B12-PE38) when the tumor size reached approximately 150 mm^3 (n = 5). Drugs were administered intravenously as indicated schedule in Fig. 5e every other day for six injections. During treatment, tumor size and body weight in mice were monitored. For survival study, mice were sacrificed when tumor size reached 2000 mm^3. To evaluate the therapeutic effect of B12-PE38 in colorectal cancers, HT29 tumor-bearing mice were randomly divided into 2 groups and treated with PBS, and B12-PE38 (0.6 mg/kg) (n = 5). The mice were treated as scheduled above for six injections. During treatment, tumor size and body weight were recorded. After treatment, the major organs including heart, liver, spleen, lung, kidney, and tumor were collected, and frozen sections were prepared and analyzed by H&E staining, Ki67 and TUNEL staining.

For combination therapy, tumor-bearing mice (PC3) received totally 8 does of immunotoxin B12-PE38 formulated at 0.4 mg/kg and 4 does of docetaxel (DTX) at 2.5 mg/kg, as demonstrated in administration schedule presented in Fig. 6a. Meanwhile, mice receiving B12-PE38 or docetaxel alone were used positive control groups, but those receiving PBS were used a negative control group. Tumor growth and volume were monitored every 2 days until tumor size reached 2000 mm^3.

Patient derived CRPC xenograft model and treatment

A piece of fresh PDX tissue (2nd passage) was generously provided by Nanchang University and confirmed to express CEACAM5 through IHC. The sample was originated from a patient diagnosed with PCa. Informed consent was obtained from the patient, and all procedures involving human samples were approved by the Medical Ethics Committee of the Shenzhen People's Hospital, Nanfang University and Nanchang University.

Upon receipt, the PDX tissues was swiftly dissected into 3 × 3x3 mm fragments on ice and implanted subcutaneously into the right forelimb of NCG mice (NOD/ShiLtJGpt-*Prkdc*^{em26Cd52}*Il2rg*^{em26Cd22}/Gpt) to propagate the tumors. Once the tumor volume reached 800 to 1000 mm^3, it was harvested, dissected into smaller fragments, and subcutaneously inoculated into the right forelimb of new NCG mice. When these tumors reached a volume of 100 mm^3, the mice were randomly assigned to four treatment groups: PBS, docetaxel (DTX), B12-PE38, and a combination of B12-PE38 and DTX. The combined treatment group received a total of 8 doses of immunotoxin B12-PE38 at a dosage of 0.4 mg/kg and 4 doses of docetaxel at a dosage of 2.5 mg/kg, as detailed in the administration schedule depicted in Fig. 6d. Tumor growth and volume were monitored every 2 days until the tumor size reached 2000 mm^3 for the purpose of anti-tumor efficacy evaluation and survival assessment, with 5 mice per group.

Mouse bone metastasis xenograft models and treatments

To establish intra-tibial bone xenograft models, PC3 cells (5×10^6) were injected directly into the tibia of mice, and the models were monitored by X-ray every 7 days until osteolytic changes in the tibial bone were detected, thereby confirming the successful establishment of the model. Once osteolytic lesions in the tibia were observed based on X-ray indications, the mice were randomly assigned to three treatment groups: PBS, B12-PE38 at 0.3 mg/kg, and B12-PE38 at 0.6 mg/kg. A total of 6 doses of the drugs were administered (Fig. 7a). During the treatment period, the intra-tibial xenografts were monitored by X-ray every 7 days. In the survival analysis, the visible signs of bone fractures, as monitored by X-ray and a weight decrease of more than 20%, were considered an endpoint for the experiment.

Statistics

All statistical analyses were performed using GraphPad 9.0 (GraphPad Software Inc., United States). Numerical data were presented as means ± standard error of mean (SEM). For more than two groups of continuous variables, one-way Anova or two-way Anova were performed to determine the difference significance among groups. Differences between two groups of variables were compared and confirmed by two-tailed Student's t-test. Survival curves were depicted using Kaplan–Meier's method and compared by the log-rank test. A $p < 0.05$ was considered as a statistically significance.

Results

Recapitulation of CEACAM5 expression in PCa cell lines and clinical samples

CEACAM5 has been revealed significant upregulation during the transformation of prostate adenocarcinoma into aggressive phenotypes following AR targeted therapies [31], implying its potential as a targeting biomarker for diagnostic and therapeutic applications in AVPC. To recapitulate the CEACAM5 expression profiles in AVPC, we first examined its expression in several PCa cell lines, and meanwhile, a colorectal cancer cell HT29 was used as a positive control which has been validated for the high level of CEACAM5 expression [32]. PCa derived cell lines maintaining AR expression including LNCAP, C4-2, 22RV1, VCAP were classified as prostatic adenocarcinoma (PRAD), but PC3, DU145 and NCI-H660 were regarded as AVPC derived cell lines. In addition, PC3 and DU145 were both regarded as DNPC lacking both neuroendocrine differentiation markers and AR transduction, but NCI-H660 was recognized as a cell line representing NEPC at terminal transformation stage [33]. Cell immunofluorescence staining confirmed the high expression of CEACAM5 in HT29, and PC3 as a DNPC cell line just mildly expressed CEACAM5. No obvious positive staining was detected in PRAD cell lines LNCAP, C4-2 and 22RV1. While DU145 is a DNPC cell line, the in vitro cell staining was disclosed negative for CEACAM5 expression, which is consistent with previous studies [17, 23] (Fig. 1a). Further flow cytometry obtained similar results, demonstrating that more than 50% HT29 and 24% PC3 cells expressed CEACAM5, and H660 as a typical NEPC cell lines showed approximate 100% positivity for CEACAM5 expression; whereas other PCa cell lines indicated undetectable expression for CEACAM5 (Fig. 1b). The loss of AR pathway transduction initiates the transformation into an aggressive phenotype and serves as a hallmark for distinguishing AVPC [34]. We measured the expression of AR with immunofluorescence staining, indicating strong expression in 22RV1 and C4-2, and negative expression for PC3, which highly aligns with their cell subtypes (Fig. S1a). Meanwhile, PSMA, a well-characterized membrane antigen of PRAD, was demonstrated high expression in PRAD cell lines LNCAP, C4-2 and 22RV1 and no expression in the AVPC derived cell line PC3 (Fig. S1b), which is consistent

with previous reports about low to absent expression of PSMA in NEPC and DNPC [14, 23].

Subsequently, CEACAM5 expression from four cases of NEPC samples, characterized with loss of prostatic adenocarcinoma characteristics (AR-) and positive staining of random neuroendocrine biomarkers (SYN or CGA) [9], unraveled that two cases showed CEACAM5 positive expression (Fig. 1c). Its expression was also identified in a patient-derived xenograft tissue from a panel of PCa PDX tissues. DNPC derived PC3-induced tumor tissues exhibited mild and noticeable expression of CEACAM5 with a heterogenous property. However, negative results for CEACAM5 staining were indicated in a series of PCa samples categorized from ISUP1 (International Society of Urological Pathology) to ISUP5, benign prostate hyperplasia and normal prostate tissues (Fig. 1d), implicating the specificity of CEACAM5 elevation in NEPC and DNPC. Likewise, staining in a tissue array including a variety of normal tissues revealed negative expression of CEACAM5 except for esophagus and colon (Fig. S2).

In summary, systematic screening of CEACAM5 on PCa cell lines and tissue samples confirmed its specific and upregulated expression in AVPC. Nevertheless, CEACAM5 expression profiles still vary among different pathological phenotypes of AVPC, and targeting CEACAM5 in certain AVPC might be a suitable option to develop therapeutics.

Nanobody B12 exhibits an excellent affinity against CEACAM5 antigen

After recapitulated the expression of CEACAM5 in AVPC, we next attempted to isolate nanobodies against CEACAM5 antigen. Human CEACAM5-Fc protein was used as a bait to conduct three-round biopanning with a naïve phage nanobody library (1×10^9 diversity) and a subtractive screening with Fc fragment was carried out to remove potential binder to Fc prior to third round screening.

After three-rounding selection, the sub-library was enriched 800 folds in colony forming units (cfu) when compared with first round (Fig. 1a), indicating that the potential binders to CEACAM5 were greatly amplified and enriched. The preliminary phage ELISA identified eight positive clones, and subsequent sequencing confirmed that a clone, designated as B12 was highly enriched (7/8) (Fig. 2b).

Next, we expressed and purified nanobody B12 protein through prokaryotic expression system and obtained B12 nanobody with high purity and solubility, and a control nanobody (ConNb) was purified as well (Fig. 2c). B12 nanobody was further confirmed through immunoblotting with antibodies for His tag, and HA tag which was integrated in the C terminal together with a cysteine for subsequent labeling (Fig. 2d). Subsequently, an ELISA assay demonstrated the superior binding activity of nanobody B12 against CEACAM5 antigen over ConNb (Fig. 2e). In parallel, a SPR assay confirmed the high binding affinity of nanobody B12 to CEACAM5 with a satisfactory dissociation constant (KD) of 66.53 nM (Fig. 2f). Consistent with results from ELISA and SPR assays, a Cell ELISA assay with IR800-labeled nanobodies further validated the marked binding ability of B12 to CEACAM5-expressing cell lines including HT29 and PC3 when compared to control nanobody (Fig. S3a and Fig. 2g). To confirm the binding specificity of B12 against CEACAM5, PC3 cells and MKN45 cells were knocked down CEACAM5 expression with targeted shRNA through lentivirus transduction (Fig. 2h and Fig. S3b). In line with CEACAM5 knockdown, B12 binding activity was significantly reduced in PC3 cells following knockdown CEACAM5 when compared with parental PC3 cells as demonstrated by Cell ELISA and dot blot assays (Fig. 2i, j). Meanwhile, consistent results were also observed in CEACAM5-knockdown MKN45 cells by both cell ELISA and dot blot assays (Fig. S3c and d). To further exclude potential cross-reactivity with other CEACAM family members that share high sequence homology, we evaluated the binding activity of B12 to

(See figure on next page.)

Fig. 1 Recapitulation of CEACAM5 expression profiles in PCa cell lines and tissues. **a** Immunofluorescence staining identified the membrane expression of CEACAM5 on DNPC derived PCa cell line PC3, but not in other PCa cell lines derived from prostatic adenocarcinoma, and HT-29 cells were used as a positive control. Scale bar, 100 μm. **b** Determination of CEACAM5 positivity in PCa derived cell lines by flow cytometry assay. The positive CEACAM5 staining was detected and confirmed in both AVPC derived PC3 and NCI-H660 cell lines, but not in cell lines derived from prostatic adenocarcinoma. The lower penal indicated CEACAM positive AVPC cell lines including NCI-H660 (100%) and PC3 (24.1%). The human colon carcinoma cell line HT29 was selected as the positive control (54.3%). The upper penal demonstrated negative CEACAM5 expression in the PCa cell lines. **c** Tissue CEACAM5 expression profiles in PCa tissue samples. Immunohistochemical assay verified the membrane expression of CEACAM5 in clinical samples (NEPC: 2/4) and PDX tissues, which were characterized by a consistent and diffuse CEACAM5 expression profile. In contrast, the expression profile of CEACAM5 in CDX samples of DNPC derived PC3 cell line was manifested as a focal and heterogenous expression profile. Scale bars, 20 μm. **d** CEACAM5 staining in prostatic adenocarcinoma (classified by ISUP grade), normal prostate tissue and benign prostatic hyperplasia. Notably, no positive staining of CEACAM5 was observed in these clinical samples. Scale bars, 250 μm

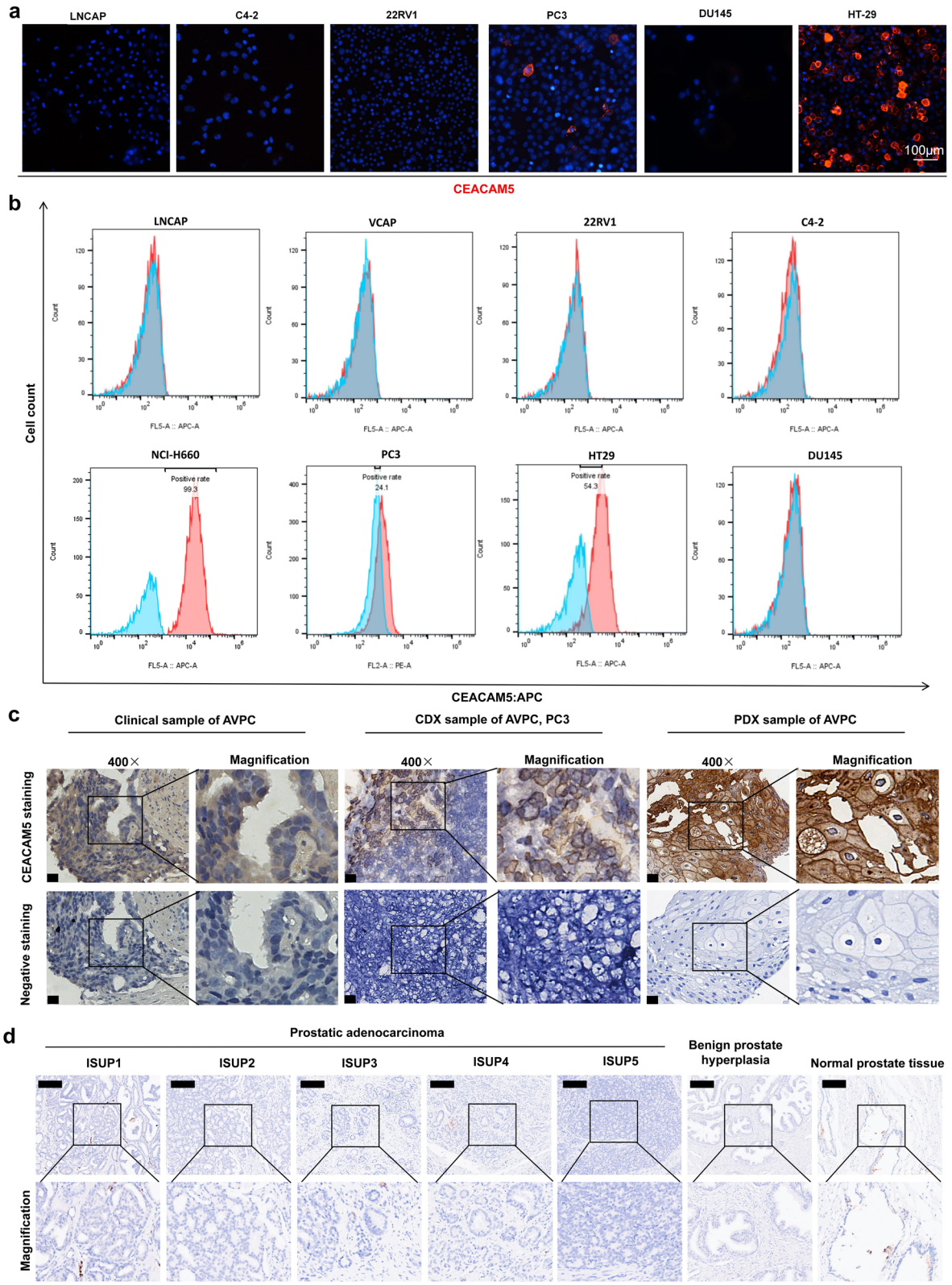

Fig. 1 (See legend on previous page.)

CEACAM1, CEACAM3, CEACAM6, and CEACAM8 using ELISA. The results showed that B12 exhibited minimal binding to CEACAM1, 3, 6, and 8, comparable to that observed with negative controls (Fc and BSA proteins). In contrast, strong binding was observed with CEACAM5 (Fig. S4). These findings disclose the high specificity of the B12 nanobody for CEACAM5, with no detectable cross-reactivity to other CEACAM family members.

Taken together, these results demonstrate that isolated B12 nanobody possesses good binding activity, high binding affinity with prominent specificity against CEACAM5, suggestive of its potential applications for designing imaging and therapeutic modalities in AVPC.

Nanobody B12 enables rapid in vivo imaging in a xenograft model induced with AVPC cells

Having demonstrating the specific expression of CEACAM5 in AVPC (NEPC and DNPC) and characterization of isolated nanobody B12, we next investigated the capability of B12 for in vivo imaging in a PC3-induced xenograft. IRDye800cw Dye (IR800), a near-infrared (NIR) dye with low background autofluorescence, good stability and high sensitivity was used to label nanobodies for in vivo imaging under NIRI window (~ 800 nM). B12 and ConNb were labeled with IR800 at the same ratio overnight and dialyzed to remove free dyes; the equal amount of B12-IR800 and ConNb-IR800 (~ 80 μg) were intravenously injected into nude mice bearing PC3 tumors. Tumor fluorescence signals were captured using the IVIS imaging system at 2, 4, 8, 12, and 24 h post systemic injection.

As shown in Fig. 3a, b, a progressive accumulation of fluorescence was observed in tumors treated with B12-IR800, reaching peak intensity at 24 h post injection. In contrast, no significant fluorescence accumulation was detected in tumors treated with ConNb-IR800. Notably, quantitative analysis demonstrated that B12-IR800 achieved approximately threefold and sixfold higher tumor accumulation compared to ConNb-IR800 at 12 and 24 h post injection, respectively (Fig. 3b). Ex vivo imaging of various organs collected 24 h after probe administration revealed that B12-IR800 predominantly accumulated in tumors, liver, and kidneys (Fig. 3c). In contrast, ConNb-IR800 was detected only in the liver and kidneys. These findings demonstrate that B12-IR800 specifically targets CEACAM5^{+} tumors, whereas ConNb-IR800 lacks this targeting capability. Quantitative analysis of organ fluorescence intensity further confirmed that tumors in the B12-IR800 group exhibited significantly stronger signals compared to those in the ConNb-IR800 group (Fig. 3d). Interestingly, livers and kidneys from mice treated with B12-IR800 also showed higher fluorescence intensity, particularly in the kidneys (Fig. 3d), which aligns with previous similar studies [18, 32]. This suggests that B12-IR800 circulating in the bloodstream or released from tumors is primarily cleared through the liver and kidneys, with the kidneys being the major route of clearance. Tissue staining with an anti-nanobody VHH antibody revealed the presence of nanobodies in tumors treated with B12-IR800, while no signal was detected in tumors treated with ConNb-IR800 (Fig. S6). This finding is in agreement with the data from both in vivo and ex vivo imaging. Notably, no nanobody signals were observed in other organs collected from B12-IR800-treated mice, despite the liver and kidneys showing strong fluorescence signals (Fig. S5). This suggests that the fluorescence observed in these organs primarily originated from the metabolism of the IR800 dye rather than the nanobodies themselves.

Collectively, these results indicate that B12 effectively enables imaging of CEACAM5-positive AVPC tumors, further supporting its potential as a nanobody for targeted drug delivery.

The B12-PE38 immunotoxin efficiently targets and inhibits CEACAM5-positive AVPC cells in vitro

Given the excellent targeting ability and specificity of B12 nanobody against CEACAM5 in vitro and in vivo, we sought to determine whether B12 nanobody could

(See figure on next page.)

Fig. 2 CEACAM5 nanobody isolation and characterization. **a** Output phage titer for three round biopanning against CEACAM5 protein. **b** Nanobody B12 sequence with three CDR domains. The whole amino acid sequence of B12 was presented and CDR domains 1, 2 and 3 were marked in red, green and blue, respectively. **c**, **d** The purification and confirmation of B12 nanobody by coomassie blue staining and immunoblotting with antibodies against HA and HIS tags. **e** The ELISA assay confirmed the superior binding activity of B12 over ConNb against CEACAM5 antigen (n = 3). Data are presented as mean ± SEM. **f** SPR assay to determine the binding dissociation constant (KD) of B12 to CEACAM5. The KD value of nanobody B12 against CEACAM5 antigen was 6.653×10^{-8} M. **g** The Cell ELISA assay to verify the binding ability of B12 to CEACAM5-expressing cells. Nanobodies were labelled with dye IR-800. Nanobody B12 was demonstrated the excellent binding ability against CEACAM5 expressing cell lines including PC3 and HT29, showing increased signals in a concentration-dependent manner over non-targeting ConNb (n = 3). Data are presented as mean ± SEM. **h** Western blot analysis of CEACAM5 knockdown efficiency in PC3 cells using targeted shRNA. **i**, **j** Cell ELISA and dot blot assays demonstrated reduced B12 fluorescence signals in CEACAM5-knockdown PC3 cells, confirming antibody specificity (n = 3). Data are analyzed by student t-test and represented with mean ± SEM; ****p < 0.0001

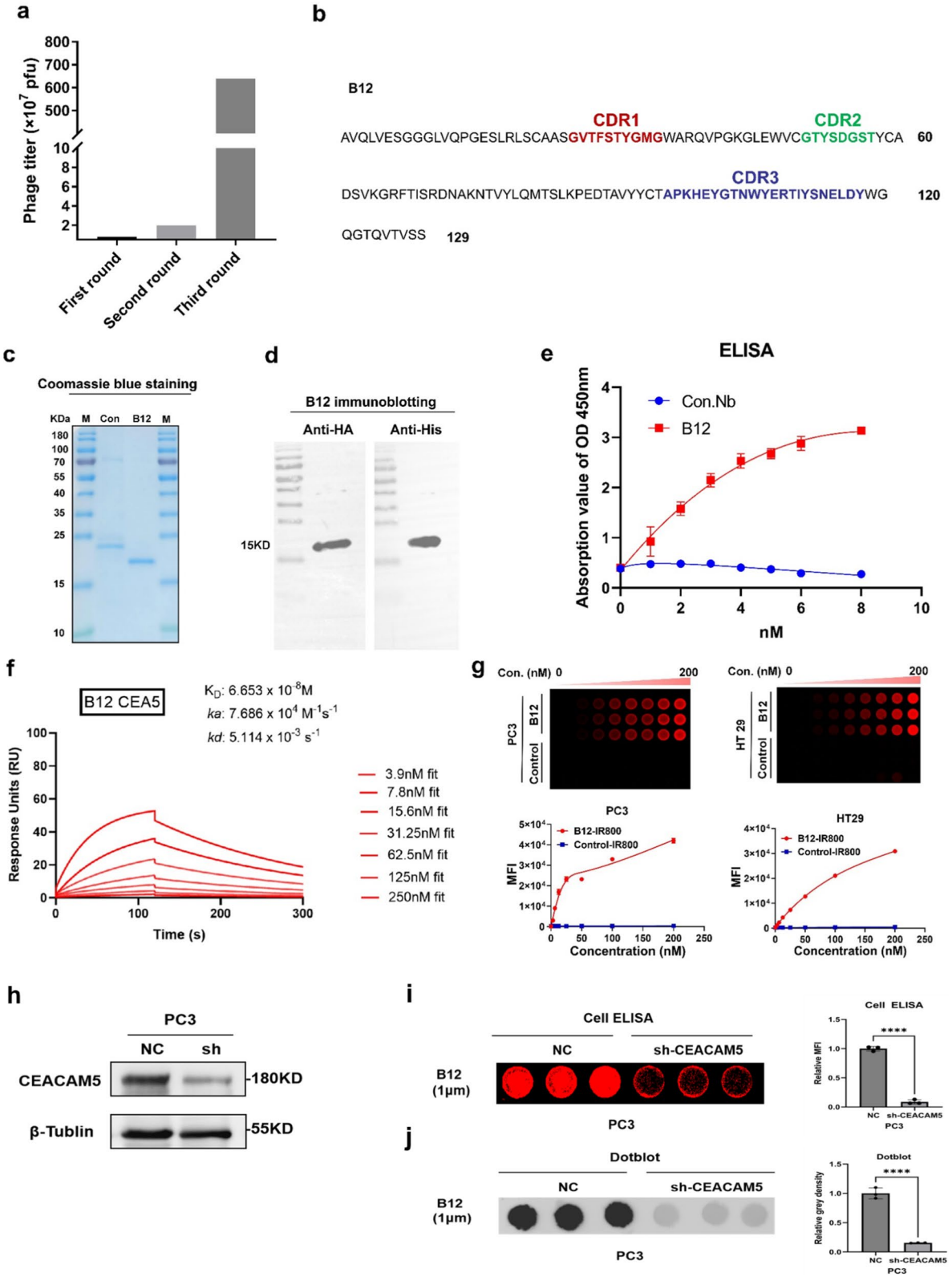

Fig. 2 (See legend on previous page.)

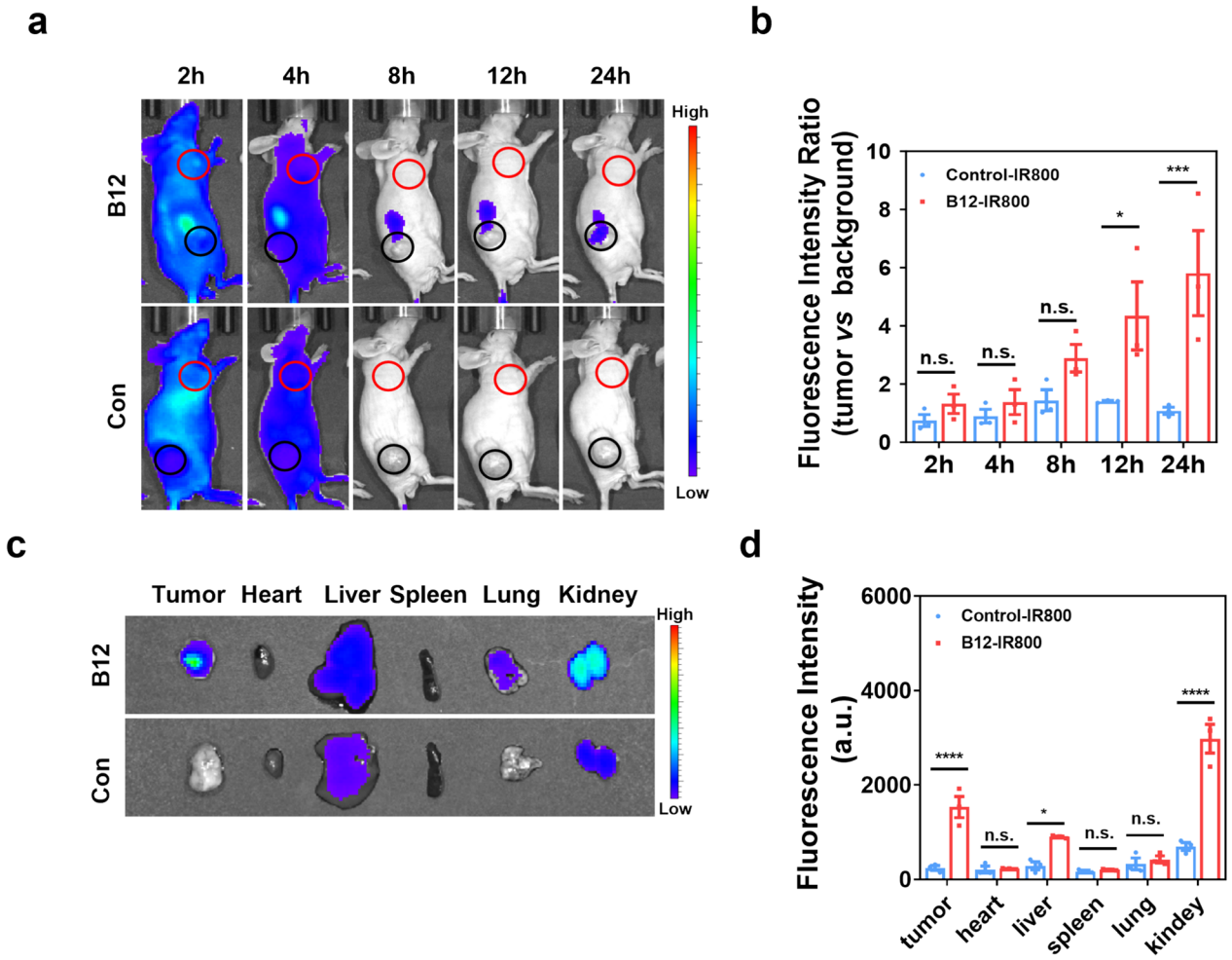

Fig. 3 B12-IR800 effectively images AVPC tumors in vivo. **a** In vivo imaging exhibited the gradual accumulation of B12-IR800 in PC3 tumors over ConNb-IR800. The most significant difference occurred at 24 h post injection. The red circles indicate the selected background areas used as fluorescence intensity references in non-tumor regions, and the black circles mark the tumor regions. **b** Quantification analysis of fluorescence intensity with tumor-to-background ratio (TBR, tumor vs background) (n = 3). Data are expressed as mean ± SEM. Statistical analysis was conducted with Student's t test. ****$p < 0.0001$; ns, not significant. TBR for B12-IR800 was significantly higher than ConNb-IR800 at 12 and 24 h post injection. **c** Ex vivo imaging on dissected various organs collected at 24 h post injection. B12-IR800 was primarily identified in tumor, liver and kidneys and Con Nb-IR800 was only observed in liver and kidneys. **d** Quantification analysis for fluorescence intensity from collected organs (n = 3). Data are expressed as mean ± SEM. *p < 0.05; **** < 0.0001; ns, not significant; Student's t test

markedly enhance the efficiency of antitumor drug by targeting CEACAM5. Immunotoxins, composed of a tumor-targeting moiety and a potent toxin with high cytotoxicity against cancer cells, have demonstrated success in the treatment of hematological malignancies and are currently being explored for their potential in treating solid tumors. For instance, Moxetumomab pasudotox, a Pseudomonas exotoxin (PE)-based immunotoxin targeting CD22 has been approved by FDA for hairy cell leukemia [35]. In this study, we engineered a CEACAM5-targeted immunotoxin by fusing the B12 nanobody with a 38-kDa fragment of PE toxin (PE38). As a negative control, an irrelevant nanobody was similarly fused with PE38. Both immunotoxins were successfully expressed and purified from a prokaryotic expression system, demonstrating high solubility and yield (Fig. 4a). ELISA assay confirmed the strong binding activity of B12-PE38 to the CEACAM5 antigen compared to ConNb-PE38 (Fig. 4b). Subsequently, the B12-PE38 was labeled with dye Cy5 to examine the binding performance in CEACAM5$^+$ cells by Cell ELISA, revealing an excellent concentration-dependent binding capability of B12-PE38-IR800 in PC3 (KD, ~ 94.48 nM) and HT-29 (KD, ~ 444.4 nM) cells; whereas no such noticeable interaction was observed in CEACAM5$^-$ 22RV1 and VCAP cells (Fig. 4c). These results indicate that PE38 toxin does not compromise

the binding ability of B12 nanobody against CEACAM5 antigen. To further validate the binding specificity, free B12 nanobodies were used to pretreat the PC3 and HT29 cells prior to B12-PE38-IR800 incubation. The data suggested that B12 could significantly disrupt the interaction of B12-PE38-IR800 with PC3 and HT29 cells, and ConNb-PE38 did not exhibit obvious binding activity to both of cells (Fig. 4d), demonstrating the good specificity of B12-PE38 to CEACAM5.

Efficient internalization and uptake of immunotoxins by cancer cells is essential to fulfill their antitumor activity. We next explored whether B12-PE38 could be internalized by CEACAM5 expressing AVPC cell lines. We demonstrated that B12-PE38 could be internalized by PC3 cells in a concentration and a time dependent manner (Fig. 4e and Fig. S6) after incubation. Similar results were also obtained by flow cytometry after the incubation of B12-PE38-Cy5 with PC3 cells (Fig. 4f). Those results implicate that B12-PE38 can be ingested by cancer cells through the interaction between B12 and CEACAM5, suggestive of the enhancement of potential antitumor activity of toxin PE38 by B12.

Subsequently, in vitro cytotoxic assay revealed that B12-PE38 did exhibit the most significantly tumor inhibitory effects in CEACAM5 expressing cell lines HT29, PC3 and MKN45) when compared to various controls including B12 alone, ConNb-PE38 or B12-PE38 mut, an inactive format of PE38 [29, 36] (Fig. 4g and Fig. S7). Moreover, EDU assay revealed that B12-PE38 also significantly decreased the proliferation of CEACAM5 expressing cell lines in HT29 and PC3, especially at a higher concentration (1.0 μM), but not B12 alone, or non-targeting immunotoxin ConNb-PE38 (Fig. 4h, i). Finally, in vitro analysis on cell migration indicated that the B12-PE38 treatment could markedly inhibit the migration of PC3 cells (Fig. 4j, k).

Collectively, these results demonstrate the excellent binding capability of immunotoxin B12-PE38 against CEACAM5 expressing cell lines as well as its potent in vitro anti-tumor efficacy.

The B12-PE38 immunotoxin effectively suppresses the progression of AVPC-derived xenografts in vivo

Owing to the highly potent cytotoxic effect of the B12-PE38 immunotoxin against CEACAM5$^+$ cancer cells including AVPC-derived PC3 cells, we further delved into its in vivo tumor inhibitory efficacy in xenograft models. Prior to in vivo antitumor exploration, it is necessary to assess the tumor targeted ability of the B12-PE38 immunotoxin with precise imaging techniques. Since the active immunotoxin is highly toxic and a large amount of immunotoxin is necessitated for in vivo imaging, the inactive format of B12-P38 mut and ConNb-PE38 mut was produced through the introduction of a single-point substitution of glutamic acid (E) with aspartic acid (D) at position 553 of PE38 protein, which significantly inactivates the toxin's enzymatic function, leading to complete loss of cytotoxic activity [36]. Totally 100 μg proteins were intravenously injected into nude mice bearing PC3 tumors after B12-P38 mut and ConNb-PE38 mut were labeled with IR800. The whole-body imaging was then captured in various time points. As indicated in Fig. 5a, b, the gradual accumulation of B12-PE38 mut-IR800 in PC3 xenograft was observed and reached the peak at 12 h post injection, whereas no such effect was found for tumors treated with ConNb-PE38 mut-IR800, suggesting that B12 nanobodies enhance the delivery efficiency of toxin PE38. Likewise, ex vivo imaging data also revealed the consistent results on excised various tissues at 24 h post injection (Fig. 5c, d), indicating that B12-PE38 mut-IR800 was significantly enriched in tumors when compared with ConNb-PE38 mut-IR800 (Fig. 5c, d). In contrast,

(See figure on next page.)

Fig. 4 The B12-PE38 immunotoxin exhibits superb in vitro binding activity and anti-tumor efficacy against CEACAM5$^+$ AVPC cells. **a** The purification of B12-PE38 and control non-targeting immunotoxin (ConNb-PE38) demonstrated by the Coomassie blue staining. **b** ELISA assay confirmed the better binding activity of B12-PE38 against CEACAM5 antigen over the non-targeting ConNb-PE38 (n = 3). Data are represented as mean ± SEM. **c** Cell ELISA assay validated the binding capability of B12-PE38 against CEACAM5 expressing cell lines including PC3 and HT29 (n = 3). The KD value of B12-PE38 against PC3 and HT29 cell lines was approximately 94.48 nM and 444.4 nM, respectively. Data are represented as mean ± SEM. **d** Pretreatment with B12 nanobodies blocked the binding activity of B12-PE38 against CEACAM5 expressing cell lines (n = 3). Data are represented as mean ± SEM. *p < 0.05; **p < 0.01; ***p < 0.001; ****p < 0.0001; One-way Anova. **e**, **f** Internalization and uptake assays for B12-PE38 in CEACAM5$^+$ AVPC derived PC3 cells. Immunotoxins were labeled with dye Cy5. The drug uptake and internalization were determined by microscopy (**e**) and flow cytometry (**f**) (n = 3). Data are represented as mean ± SEM. One-way Anova was used to analyze the difference among difference groups. *p < 0.05; **p < 0.01; ***p < 0.001; ****p < 0.0001; ns, no significance. **g** In vitro cytotoxic assay by CCK8 revealed that the B12-PE38 immunotoxin significantly reduced the viability of cancer cells expressing CEACAM5, but not the B12 nanobody alone, inactive immunotoxin B12-PE38 mut or non-targeting ConNb-PE38 (n = 3). Data are represented as mean ± SEM. Two-way Anova was used to analyze the difference among difference groups. *p < 0.05; **p < 0.01. **h**, **i** EDU staining and quantification after various treatments, implying that B12-PE38 inhibits the proliferation in CEACAM5$^+$ cell lines including PC3 and HT29 (n = 3). Data are represented as mean ± SEM. One-way Anova; *p < 0.05; **p < 0.01; ***p < 0.001; *p < 0.0001; ns, no significance. **j**, **k** In vitro migration assay indicated that B12-PE38 can efficiently suppress the migration of CEACAM5$^+$ cell line PC3 (n = 3); scale bars: 50 μm. Data are represented as mean ± SEM. One-way Anova; *p < 0.05; ns, no significance

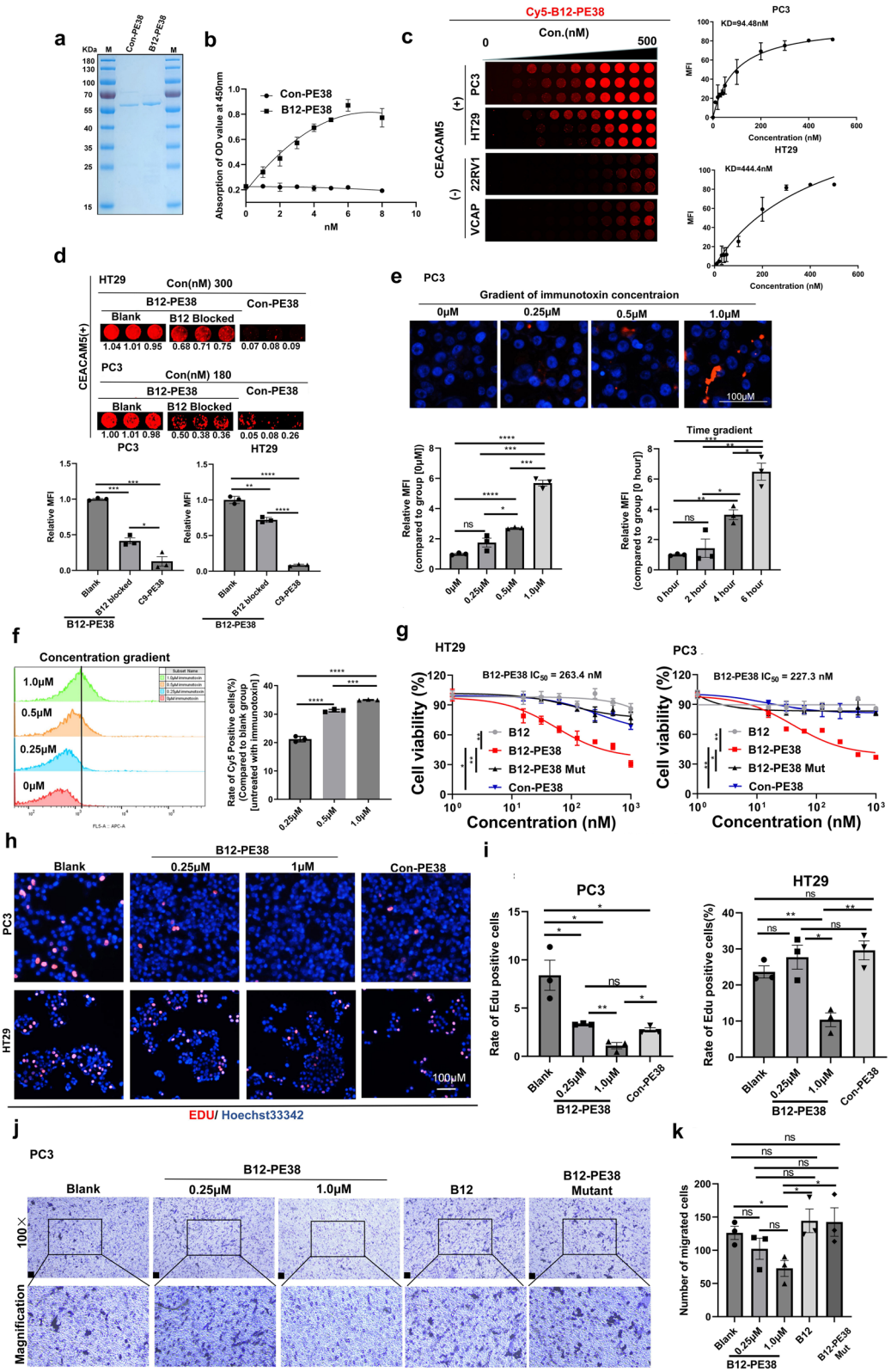

Fig. 4 (See legend on previous page.)

ConNb-PE38 mut-IR800 was primarily observed in liver and kidneys (Fig. 5c, d). Fluorescence staining in tumor tissues by an anti-VHH antibody recognizing nanobody frameworks verified the noticeable presence of B12-PE38 mut over ConNb-PE38 mut (Fig. S8). These results demonstrate the in vivo targeting capability of the immunotoxin B12-PE38 in PC3 tumors.

Next, the in vivo anti-tumor efficacy of the immunotoxin B12-PE38 against PC3 xenografts was investigated. Two doses of B12-PE38 (0.4 and 0.6 mg/kg) were selected for tumor treatment in PC3 tumor-bearing mice, and PBS and B12 nanobodies were used as controls; mice were treated as scheduled in Fig. 5e. The significant anti-tumor efficacy was observed in the both groups receiving two doses of the immunotoxin B12-PE38 with a slightly better inhibition for the higher dose (Fig. 5f–h). However, PBS or B12 nanobodies alone did not indicate any tumor suppression effect (Fig. 5f–h). Moreover, H&E staining in various organs collected from different groups did not disclose notable morphological alternation; blood routine and biochemistry analyses also indicated no significant difference among groups receiving either control or immunotoxin treatments (Fig. S9, S10). These results manifest that B12 nanobodies efficiently improve the antitumor activity of PE38 toxin through CEACAM5 targeting and enhance its biosafety.

Furthermore, immunostaining with Ki67 antibodies and TUNEL assay demonstrated that B12-PE38 immunotoxin resulted in the inhibition of cell proliferation ($Ki67^+$) and the induction of cell apoptosis ($TUNEL^+$) in a dose-dependent manner when compared with control groups (Fig. S11).

Owing to the broad investigations of $CEACAM5^+$ in the malignances of gastrointestinal system, it is worthwhile to evaluate the anti-tumor efficacy of B12-PE38 against these cancers with the CEACAM5 expression. Indeed, the B12-PE38 immunotoxin (0.4 mg/kg) delayed the HT29 tumor growth and markedly extended the mice survival (Fig. 5i, j and Fig. S12), indicating its potent anti-tumor potential in other $CEACAM5^+$ tumors in addition to AVPC tumors.

Taken together, these results reveal that targeting CEACAM5 using B12 nanobodies can enhance the delivery efficiency of the antitumor toxin PE38, and strengthen in vivo anti-tumor efficacy of immunotoxin against AVPC-derived xenografts and other $CEACAM5^+$ cancers, highlighting great promise for potential translation.

The B12-PE38 immunotoxin improves the anti-tumor efficacy of docetaxel to inhibit $CEACAM5^+$ PCa progression in CDX and PDX models

Currently, docetaxel-based chemotherapy remains the first-line recommendation for metastatic castration-resistant prostate cancer (mCRPC) and metastatic hormone-sensitive prostate cancer (mHSPC), but its efficacy is limited as a monotherapy. Combination therapy has been clinically exploited as a key strategy to improve therapeutic efficacy [37]. Thus, combination regimens of docetaxel with other standard of care in different prostate cancer subtypes have been tested in clinical trials and achieved more durable tumor remission, demonstrating significant benefits for patients, including those with AVPC [38, 39]. Building on these clinical findings, it is important to assess the combinational anti-tumor efficacy of the B12-PE38 immunotoxin with docetaxel in AVPC-derived tumor models. To this end, PC3 tumor-bearing mice were treated with B12-PE38 (0.4 mg/kg), docetaxel (2.5 mg/kg), or their combination according to the schedule outlined in Fig. 6a. The results showed that B12-PE38 and docetaxel alone produced similar tumor inhibitory effects on PC3 tumor growth under the indicated treatment schedule; however, the combination treatment suggested the most significant tumor suppression among four groups (Fig. 6b and Fig. S13a). Both drugs, administered as monotherapies, extended

(See figure on next page.)

Fig. 5 In vivo tumor targeting capability and anti-tumor efficacy of the immunotoxin B12-PE38 against $CEACAM5^+$ xenografts. **a**, **b** The whole-body imaging and quantification of mutant immunotoxin B12-PE38 in AVPC derived PC3 xenografts. Approximately 100 μg of dye-labeled B12-PE38 mut and non-targeting ConNb-PE38 mut were systemically injected into tumor bearing mice and tumor images were collected in various time points (n = 3). The red circles indicate the selected background areas used as fluorescence intensity references in non-tumor regions, and the black circles mark the tumor regions. Data are expressed as mean ± SEM. Student's t test; $^{**}p < 0.01$; $^{****}p < 0.0001$; ns, not significant. **c**, **d** Ex vivo organ imaging and quantification for B12-PE38 mut and non-targeting ConNb-PE38 mut 24-h post-injection (n = 3). Data are expressed as mean ± SEM. Student's t test; $^{**}p < 0.01$; $^{****}p < 0.0001$; ns, not significant. **e** Treatment schedule of immunotoxin in PC3 tumor-bearing mice. **f**, **g** Tumor growth curve of PC3 tumors receiving the two different doses of immunotoxin B12-PE38 as well was B12 alone or PBS (n = 5). Data are expressed as mean ± SEM. Two-way Anova analysis was conducted to assess the difference among groups. $^{**}p < 0.01$; $^{***}p < 0.001$; $^{****}p < 0.0001$; ns, not significant. The immunotoxin B12-PE38 significantly reduce the growth of PC3 xenograft, but no inhibition was observed in xenograft receiving B12. **h** Tumor weight from different treatment groups (n = 5). Data are expressed as mean ± SEM. One-way Anova; $^{**}p < 0.01$. **i** The anti-tumor efficacy of B12-PE38 against HT29 xenografts (n = 5). Data are expressed as mean ± SEM. Two-way Anova analysis; $^{****}p < 0.0001$. **j** Survival analysis of mice bearing HT29 tumors receiving B12-PE38 treatment. The difference between two groups was assessed by Kaplan–Meier survival analysis (log-rank test); $^{**}p < 0.01$

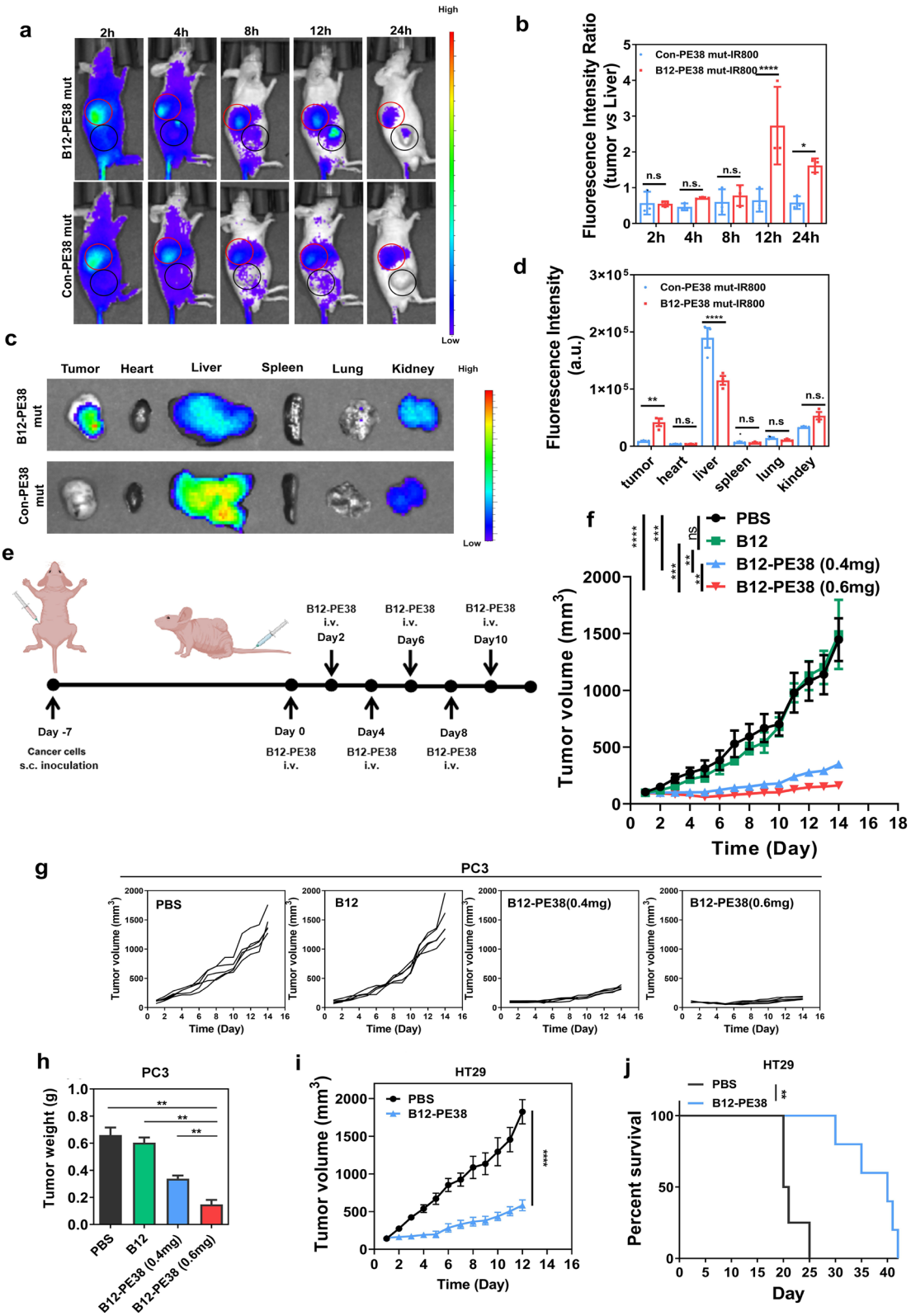

Fig. 5 (See legend on previous page.)

the lifespan of tumor-bearing mice, with B12-PE38 showing a slightly superior response. However, the combination regimen achieved the best overall survival outcomes (Fig. 6c).

Patient-derived xenograft models represent an invaluable and powerful tool for the preclinical evaluation of novel therapeutic agents, bridging the gap between laboratory research and clinical application. In this study, we screened a panel of prostate cancer samples with CEACAM5 staining and identified a patient with prostate cancer that, while not a typical AVPC, exhibited high CEACAM5 expression. Due to the challenges associated with obtaining fresh clinical samples from typical AVPC cases, and as a proof of concept, we established a PDX model using this prostate tumor sample. This model was then employed to investigate the antitumor efficacy of B12-PE38, both as a monotherapy and in combination with docetaxel as illustrated in Fig. 6d. Consistent with the PC3 CDX model, monotherapies for both drugs significantly inhibited the PDX tumor progression while no difference between them; the best tumor repression was achieved with the combination treatment, indicating the prominent combinational efficacy of B12-PE38 and docetaxel (Fig. 6e and Fig. S13b). In addition, the combination regimen also markedly prolonged the mice survival when compared with either monotherapy in which survival was also extended (Fig. 6f).

Collectively, our findings demonstrate that the B12-PE38 immunotoxin enhances the anti-tumor efficacy of docetaxel and effectively delays the progression of CEACAM5$^+$ prostate cancers in both an AVPC-derived CDX model and a PDX model, indicative of strong potential for clinical translation.

The B12-PE38 immunotoxin effectively inhibits bone metastatic lesions derived from AVPC cells

Advanced PCa often metastasizes to adjacent and distant sites; among them, bone is the most frequent metastatic site for advanced PCa, especially for CRPC [40]. Currently, bone metastasis of PCa is incurable and is a leading cause for the cancer-related death, highlighting the importance to develop new therapeutic strategies. Given the exceptional antitumor performance of the B12-PE38 immunotoxin in CEACAM5$^+$ CDX and PDX models, we sought to determine whether it can decelerate the progression of bone metastasis initiated by AVPC-derived cells. To this end, a bone metastatic model through direct intra-tibial injection of PC3 cells was constructed. Two doses of B12-PE38 (0.3 and 0.6 mg/kg) was administered, and tumor suppression efficacy was evaluated through X-ray imaging (Fig. 7a). Metastatic mice with noticeable osteolytic lesions and visible signs of pathological bone fracture were considered to have reached the endpoint and were euthanized accordingly. We found that both doses of B12-PE38 could significantly delay the development of bone metastasis, with the higher dose (0.6 mg/kg) demonstrating superior efficacy compared to the lower dose (0.3 mg/kg); whereas vehicle control did not show any inhibitory effect on bone metastasis, leading to pathological bone fracture in 67% tumor-bearing mice (4/6) (Fig. 7b). Further CT scanning and bone reconstruction for the collected tibias revealed that both doses of B12-PE38 significantly improved the bone conditions across multiple parameters including bone integrity, mineral density, bone surface and volume, tumor reduction, and the ratio of bone to tumor (Fig. 7c–i). The higher dose of B12-PE38 (0.6 mg/kg) showed greater improvements than the lower dose in bone mineral density, bone volume and the ratio of bone to tumor (Fig. 7d–i). In addition, pathological analysis of the tibias also suggested a dose-dependent improvement of the ratio of tumor to bone marrow (Fig. 7j, k).

Taken together, our findings indicate that the B12-PE38 immunotoxin significantly delays the progression of bone metastatic lesions initiated by AVPC-derived cells, underscoring its strong potential as a therapeutic option for managing the lethal bone metastases associated with advanced PCa.

Discussion

AVPC lacking adenocarcinoma characteristics, resists most of standard of care for advanced PCa and rapidly progresses into lethal terminal stage [34, 41]. Thus, it is an urgent need to develop novel imaging and therapeutic

(See figure on next page.)

Fig. 6 The combinational anti-tumor efficacy of the B12-PE38 immunotoxin with docetaxel against CEACAM5$^+$ prostate cancers. **a** The treatment schedule for combination treatment of B12-PE38 with docetaxel in a PC3-derived CDX model. **b** Tumor growth curves among different groups to examine the combinational anti-tumor efficacy of the immunotoxin B12-PE38 with docetaxel against PC3 tumors (n = 5). Data are presented as mean ± SEM. Statistical analysis was performed by Two-way Anova test; $^{**}p < 0.01$; $^{***}p < 0.001$; ns, not significant. **c** Survival study for the combination treatment of B12-PE38 with docetaxel in a PC3-derived CDX model. Statistical assessment for the survival curves was conducted with Kaplan–Meier survival analysis (log-rank test); $^{*}p < 0.05$; $^{**}p < 0.01$; ns, not significant. **d** The treatment schedule for combination treatment of B12-PE38 with docetaxel in a CEACAM5$^+$ PDX model. **e** PDX tumor growth curves after the combination treatment (n = 5). Data are presented as mean ± SEM. Two-way Anova; $^{***}p < 0.001$; $^{****}p < 0.0001$; ns, not significant. **f** Kaplan–Meier survival analysis for the combination treatment (n = 5). $^{**}p < 0.01$; $^{***}p < 0.001$; ns, no significance; log-rank test

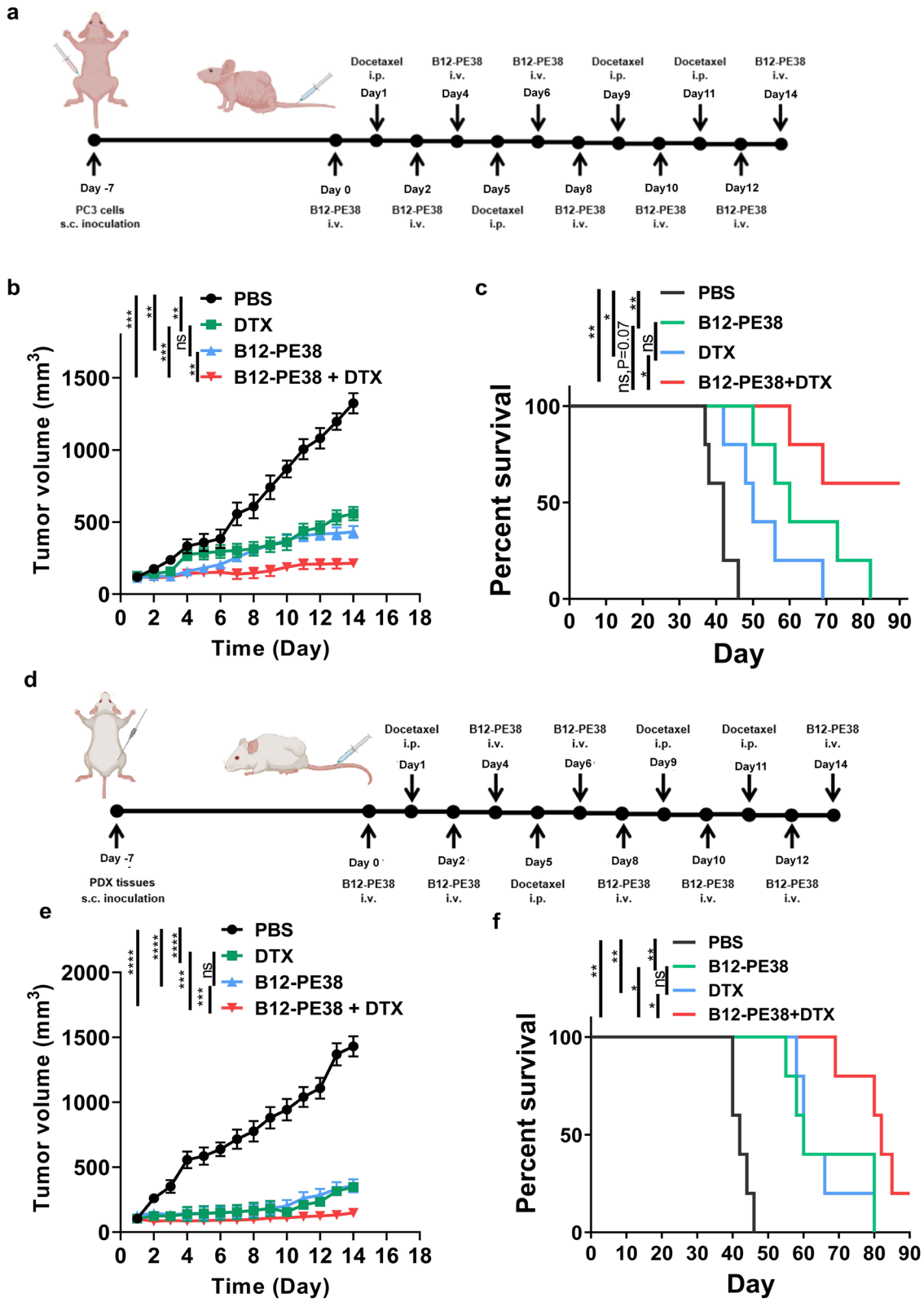

Fig. 6 (See legend on previous page.)

strategies for management of advanced PCa including AVPC. Targeting cancer surface markers to design diagnostic and therapeutic modalities is an effective and feasible strategy, especially for drug resistant tumor clones arised from phenotype transformation [42]. PSMA, a surface marker highly expressed in the most prostate cancer cells, has been demonstrated as an targetable membrane protein for PCa. A variety of modalities have been tested in preclinical and clinical settings with 177Lu-PSMA-617 which was approved to treat those patients with mCRPC following treatment with a prior androgen receptor signaling inhibitor (ARSI) and taxane chemotherapy [43]. However, the expression of PSMA is usually lost or significantly down-regulated in CRPC, especially in NEPC and DNPC, possibly due to the dysregulated AR pathway transduction [13, 16, 44, 45]. Likewise, diminished expression of TROP2 and PSCA are also observed in clinical samples of AVPC [13, 14]. DLL3, another important membrane protein in prostate cancer cells, is overexpressed in NEPC with a satisfying positive rate around 80% [46, 47], but a limited expression is identified in DNPC [13].

CEACAM5, a membrane protein which has long been extensively investigated in malignancies of gastrointestinal tract as a diagnostic and therapeutic target, was also demonstrated the more prominent and higher expression in NEPC than PSMA, PSCA, Trop2 and DLL3 [13, 15]. More importantly, it was further verified the high expression in DNPC [13, 14]. These findings make CEACAM5 an ideal target candidate for formidable AVPC. Given that multiple modalities directed CEACAM5 have been or are being tested in clinical trials, it is feasible for them to rapidly be applied for the treatment to CEACAM5$^+$ AVPC. Nevertheless, the majority of CEACAM5-targeted agents harness full-length antibodies to achieve tumor homing and drug delivery. Due to the large molecular size, full-length antibody-based drugs often result in insufficient tissue penetration, long half-life and non-specific side effect initiated by Fc fragment [15, 22, 25, 26, 28]. For instance, full-length antibody-based radiotracer probe for PET imaging normally require three to four days to accumulate in tumors and achieve optimal imaging results [19, 20]. This extended time frame can pose potential radioactive risk to patients or medical personnel. In contrast, nanobodies, derived from single-domain antibodies, are considered as the smallest functional antibodies with approximately molecular weight of 15 kD. They offer several advantages, including enhanced stability, high binding affinity, low immunogenicity, excellent tissue penetration, rapid clearance, easy engineering, and efficient production with microbial systems [48, 49], all of which make them a highly attractive focus area for drug development. Since the approval of Caplacizumab, the first nanobody-based drug, in 2018, several other nanobody-based therapies, such as Ozoralizumab and Ciltacabtagene autoleucel, have entered clinical use, with many more advancing through industrial pipelines [49]. These developments underscore the growing impact of nanobody technology in modern medicine. Targeting CEACAM5 with nanobodies has been demonstrated a promising potential for cancer imaging and therapy, including nanobody-based immuno-PET, nanobody drug conjugates, nanobody-mediated NIRII imaging and surgery guidance, T cell engagers, etc. [17, 18, 21, 32, 50]. Given the high expression of CEACAM5 in AVPC with limited therapeutics, we isolated and obtained the B12 nanobody against CEACAM5, which specifically recognizes CAECAM5$^+$ AVPC or colorectal cancer cells with high binding activity. We demonstrate that B12 conjugated with fluorescent dye IR800 enables rapid tumor imaging in an AVPC-derived xenograft model within 24 h after administration, significantly faster than three to four days typically required for conventional full-length antibodies. This finding implicates that same-day imaging for AVPC tumors is feasible in the clinical setting when the B12 nanobody is labeled with a radiotracer for immuno-PET after optimization. The rapid clearance of nanobodies makes them particularly well-suited to same-day imaging, which is highly desirable in clinical practice. On the other hand, the rapid imaging property can expedite the identification of CEACAM5$^+$ AVPC patients, which is the prerequisite for targeting CEACAM5 therapy.

(See figure on next page.)

Fig. 7 The B12-PE38 immunotoxin effectively inhibits the progression of bone lesions induced by AVPC-derived cells. **a** Treatment schedule in PC3-induced tibial bone metastatic model. Drug administration started at 3 weeks after intra-tibial implantation of PC3 cells when X ray identified the local osteolytic lesions. Totally, six doses of B12-PE38 were administered every other day. **b** The X ray imaging for monitoring tibial bone lesions during the treatment (n = 6). The red cross indicated the visible signs of bone fracture and reached the endpoint of experiment. **c** CT scanning and bone reconstruction in three groups. **d**–**i** Multiple parameters to assess bone conditions, including bone mineral density (**d**), bone surface (**e**), bone volume (**f**), tumor volume (**g**), tumor surface (**h**), bone-to-tumor ratio (**i**) (n = 6). Data are presented as mean ± SEM (n = 6). *p < 0.05; **p < 0.01; ***p < 0.001; ****p < 0.0001; ns, not significant, One-way Anova. **j** Pathological examination by H&E staining to assess the area ratio of tumor (T) to bone marrow (BM) in tumor-bearing tibial (n = 3). B, bone tissues; scale bars, 250 μm. **k** Quantification analysis for area ratio of tumor (T) to bone marrow (BM) in **J** (n = 3). Data are expressed as mean ± SEM. *p < 0.05; **p < 0.01; One-way Anova

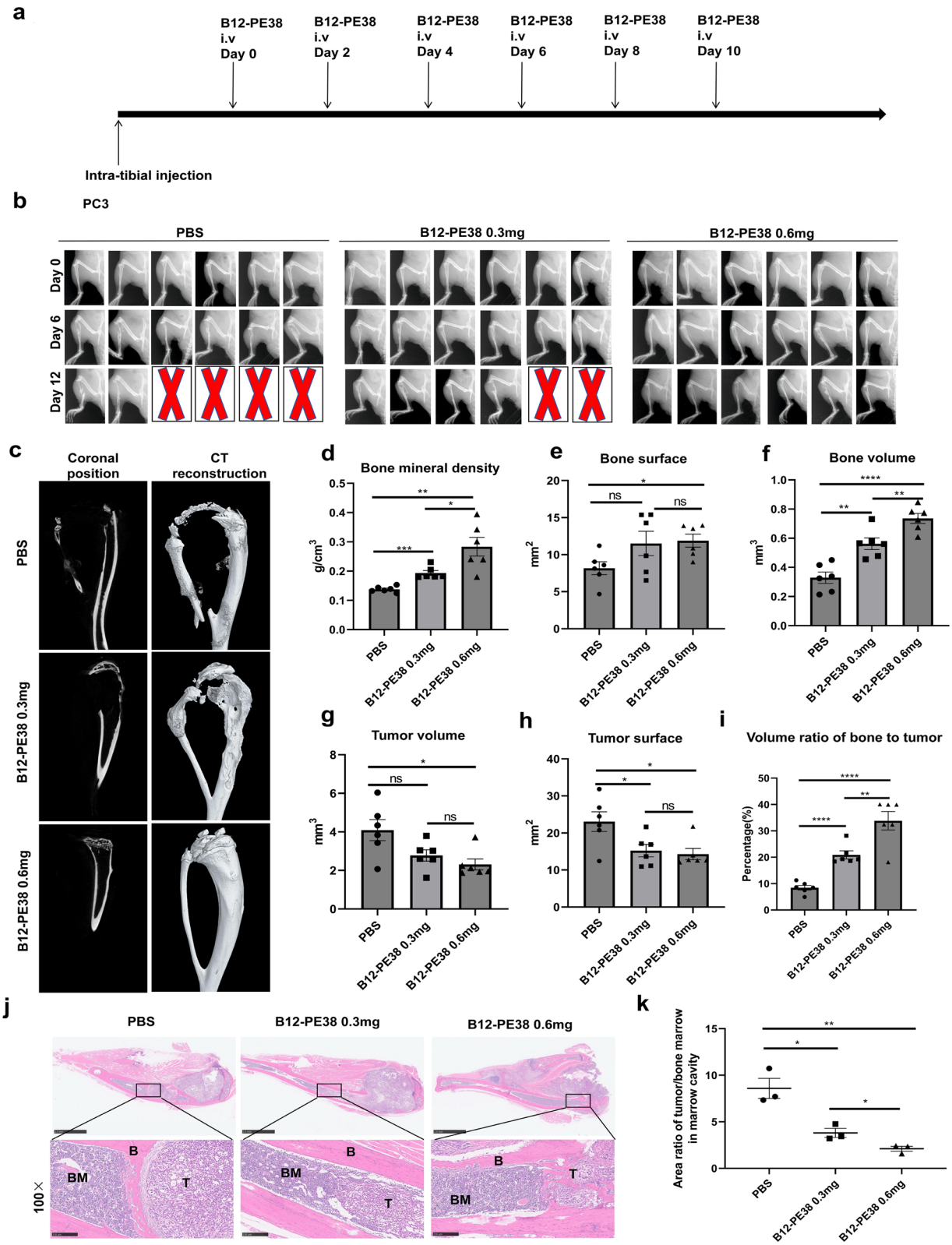

Fig. 7 (See legend on previous page.)

Immunotoxins leverage the specificity of tumor-targeting molecules, such as antibodies or nanobodies, fused with potent cytotoxic agents like Pseudomonas exotoxin A (PE-38) to selectively kill cancer cells while sparing normal tissue. Moxetumomab pasudotox (Moxe), an PE38-based recombinant immunotoxin (RITs) targeting CD22, was approved by the FDA in 2018 to treat relapsed/refractory hairy cell leukemia (HCL) [51], highlighting the feasibility of immunotoxins for cancer therapy. However, solid tumors often pose a significant challenge for therapeutics that are effective against blood cancers, and limited responses are frequently observed with recombinant immunotoxins. Single-chain fragment antibodies (scFv) are often utilized to construct the conventional immunotoxins, resulting in relatively large recombinant proteins when fused with toxins. Like full-length antibodies, the large size of RITs may restrict their penetration and accessibility to solid tumors; replacing the scFvs with smaller nanobodies offers a potential solution to improve the accessibility of RITs to solid tumors. Meanwhile, the hydrophobic property of scFv makes RITs difficult to be purified in soluble form from E. coli. As a result, the denaturation has to be applied for RIT purification and refolding the RITs is required to restore their activity. The complexity of this procedure for RITs purification is low efficiency and cost-effective, and the activity of RITs might also be compromised. However, nanobody-based immunotoxins can be purified in soluble form with high expression levels and production yield in E. coli and refolding process is avoidable [30, 52], which helps preserve the activity of RITs to the greatest extent. Previously, a RIT composed of PSMA-targeted scFv fused with PE40 was tested in a prostate cancer xenograft model in combination with Bcl-2 inhibitor ABT-737, demonstrating a significant extension of mice survival [53]. In this study, we determined the antitumor efficacy of the immunotoxin comprised of B12 nanobody-fused PE38 in CEACAM5$^+$ AVPC and colorectal cancer models, indicating its excellent tumor homing ability and significant tumor suppressive activity without notable side effects. As a proof of concept, a PDX model derived from a patient with CEACAM5$^+$ prostate cancer also confirmed the antitumor effect of B12-PE38. Meanwhile, we demonstrate the enhanced antitumor efficacy of B12-PE38 in combination with docetaxel in both CDX and PDX models of PCa, suggesting that it is feasible to add B12-PE38 to the current standard regimens for advanced PCa. To the best of our knowledge, this is the first study to design a nanobody-based immunotoxin to treat CEACAM5$^+$ AVPC in the preclinical models.

Additionally, bone metastasis, a common occurrence for advanced PCa, is lethal and incurable as well. To date, there is no effective therapeutics to treat bone metastasis of advanced PCa or to markedly benefit patients with bone metastasis. In this study, we demonstrate that the B12-P38 immunotoxin inhibits the progression of PC3-induced intra-tibial tumors which mimic the bone metastasis. This finding underscores the strong potential to treat bone metastasis through targeting CEACAM5. Since a variety of modalities targeting CEACAM5 developed for other epithelial malignancies are available, evaluating these therapeutics in CEACAM5$^+$ bone metastatic lesions is highly encouraged.

The inhibition of protein synthesis is considered as a primary mechanism of action for PE38-based immunotoxins, which finally results in cancer cell apoptosis. However, recent studies have disclosed that besides the cell apoptosis, immunotoxins induce immunogenic cell death (ICD), one of programmed cell death formats which can activate innate immune cells and modulate the tumor microenvironment [54]. Clinical investigations also found a delayed antitumor response in MOC31PE-treated cancer patients, possibly mediated by ICD induction [55]; the combination of mesothelin-targeted immunotoxin with PD-1 antibodies enhanced the antitumor efficacy, further indicating the reprogramming of TME [56]. Anti-mesothelin immunotoxin has further been demonstrated to enhance the infiltration of T cells and B cells, and to promote the induction of tertiary lymphoid structures in tumors, reminiscent of an immune-active TME. In this study, owing to the utilization of immunocompromised mice, we cannot delve into immune profiles after B12-PE38 treatment, which is warranted for future investigations. Nevertheless, our study demonstrates the great potential for CEACAM5-targted immunotoxin to treat AVPC or related bone metastasis.

Conclusions

In summary, we isolated a nanobody B12 with high affinity against CEACAM5 antigen which shows high expression levels in the cancer cells of AVPC. B12 nanobodies conjugated with fluorescent dyes enable rapidly to image CEACAM5$^+$ AVPC tumors. The B12-PE38 immunotoxin efficiently accumulates into CEACAM5$^+$ tumors and effectively inhibits the progression of CEACAM5$^+$ AVPC and colorectal cancers. The combination regimen of B12-PE38 and docetaxel exhibits the enhanced tumor repression in both CEACAM5$^+$ CDX and PDX models of PCa. Finally, we demonstrate the high potency of the B12-PE38 immunotoxin against bone metastasis of PCa in a xenograft model. Our findings provide crucial insights that targeting CEACAM5 with nanobodies is an effective strategy to manage AVPC and bone metastasis, and the nanobody-based immunotoxin represents a prospective therapy for refractory AVPC, necessitating the future clinical investigation.

Supplementary Information

The online version contains supplementary material available at https://doi.org/10.1186/s12951-025-03600-x.

Supplementary material 1.

Acknowledgements
Not applicable.

Author contributions
ZJL, SCZ and JGW designed and supervised the study. ZMX, JBM, JPC and TX performed the experiments. YQH collected patient samples and gathered detailed clinical information. LHZ, GWS, ZFL, YL, CMQ, YQH, CW, JX and HBJ analyzed the data. ZMX and JPC wrote the manuscript. ZJL and SCZ revised the manuscript.

Funding
This study was supported by the National Key R&D Program of China (2023YFE0204500), the National Natural Science Foundation of China (82373775; 32101219; 82103140), and the International Science and Technology Cooperation for Shenzhen Technology Innovation Plan (GJHZ20240218114508015), Shenzhen Medical Research Fund (D2403013 and B2302051), Shenzhen Science and Technology Innovation Committee (RCBS20210706092213007), the Scientific and Technological Innovation Project of China Academy of Chinese Medical Sciences (CI2023D003, CI2021B014, and CI2023D008), the CACMS Innovation Fund (CI2023E002, CI2021A05101, and CI2021A05104), the Science and Technology Foundation of Shenzhen (Shenzhen Clinical Medical Research Center for Geriatric Diseases), the Shenzhen Science and Technology Innovation Committee (SZSTI) (RCYX20221008092950121), the Natural Science Foundation of Top Talent of SZTU (GDRC202125), the Shenzhen Science and Technology Innovation Commission (JCYJ20200109120205924), Shenzhen Key Medical Discipline Construction Fund (SZXK046), Shenzhen Governmental Sustainable Development Fund (KCXFZ20201221173612034), Shenzhen key Laboratory of Kidney Diseases (ZDSYS201504301616234), Shenzhen Fund for Guangdong Provincial High-level Clinical Key Specialties (SZGSP001), Shenzhen People's Hospital Fund (SYWGSCGZH202405 and SYWGSJCYJ202201), and Natural Science Foundation of Top Talent of SZTU (GDRC202125).

Data availability
All data relevant to the study are included in the article or uploaded as supplementary information.

Declarations

Ethics approval and consent to participate
The research was approved by the Ethics Committee of the Fifth Affiliated Hospital of Southern Medical University (2024MNWK-K-001), the Shenzhen People's hospital (AUP-230224-LZJ-543-01) and Nanchang University (BR/AF/SG-04/1.0-202112).

Consent for publication
All subjects have written informed consent.

Competing interests
The authors declare no competing interests.

Author details
[1]Department of Urology, The Third Affiliated Hospital of Southern Medical University, Guangzhou 510500, China. [2]Department of Urology, Nanfang Hospital, Southern Medical University, Guangzhou 510515, China. [3]Department of Critical Care Medicine, Guangdong Provincial Clinical Research Center for Geriatrics, Shenzhen Clinical Research Centre for Geriatrics, Shenzhen People's Hospital (the First Affiliated Hospital, Southern University of Science and Technology, the Second Clinical Medical College, Jinan University), Shenzhen 518020, China. [4]Department of Urology and Guangdong Key Laboratory of Urology, First Affiliated Hospital of Guangzhou Medical University, Guangzhou 510120, China. [5]Department of Neurosurgery & Medical Research Center, Shunde Hospital, Southern Medical University (the First People's Hospital of Shunde Foshan), Guangzhou 528308, China. [6]School of Chemistry and Chemical Engineering, Shanxi Datong University, Datong 037009, Shanxi, China. [7]Center of Laboratory Animal Science, Nanchang University, Nanchang 330031, China. [8]Key Laboratory of New Drug Evaluation and Transformation of Jiangxi Province, Nanchang 330031, China. [9]Department of Chemistry, Hong Kong University, Hong Kong, China. [10]Center for Drug Research and Development, Guangdong Provincial Key Laboratory for Research and Evaluation of Pharmaceutical Preparations, Guangdong Pharmaceutical University, Guangzhou 510006, China. [11]State Key Laboratory for Quality Ensurance and Sustainable Use of Dao-di Herbs, Artemisinin Research Center, Institute of Chinese Materia Medica, China Academy of Chinese Medical Sciences, Beijing 100700, China. [12]Department of Oncology, The Affiliated Hospital of Southwest Medical University, Luzhou 646000, China. [13]Department of Traditional Chinese Medicine and School of Pharmaceutical Sciences, Southern Medical University, Guangzhou 510515, China. [14]State Key Laboratory of Antiviral Drugs, School of Pharmacy, Henan University, Kaifeng 475004, China. [15]Department of Urology, The Fifth Affiliated Hospital, Southern Medical University, Guangzhou 510900, China.

Received: 19 February 2025 Accepted: 14 July 2025
Published online: 18 July 2025

References

1. Paolieri F, et al. Front-line therapeutic strategy in metastatic hormone sensitive prostate cancer: an updated therapeutic algorithm. Clin Genitourin Cancer. 2024;22(4):102096.
2. Belderbos BPS, et al. Novel treatment options in the management of metastatic castration-naïve prostate cancer; which treatment modality to choose? Ann Oncol. 2019;30(10):1591–600.
3. Davis ID, et al. Enzalutamide with standard first-line therapy in metastatic prostate cancer. N Engl J Med. 2019;381(2):121–31.
4. Yamada Y, Beltran H. The treatment landscape of metastatic prostate cancer. Cancer Lett. 2021;519:20–9.
5. Wang Y, et al. Mechanisms of enzalutamide resistance in castration-resistant prostate cancer and therapeutic strategies to overcome it. Br J Pharmacol. 2021;178(2):239–61.
6. Parent EE, et al. (177)Lu-PSMA therapy. J Nucl Med Technol. 2022;50(3):205–12.
7. Emmett L, et al. [(177)Lu]Lu-PSMA-617 plus enzalutamide in patients with metastatic castration-resistant prostate cancer (ENZA-p): an open-label, multicentre, randomised, phase 2 trial. Lancet Oncol. 2024;25(5):563–71.
8. Mulders PF, et al. Targeted treatment of metastatic castration-resistant prostate cancer with sipuleucel-T immunotherapy. Cancer Immunol Immunother. 2015;64(6):655–63.
9. Manucha V, Henegan J. Clinicopathologic diagnostic approach to aggressive variant prostate cancer. Arch Pathol Lab Med. 2020;144(1):18–23.
10. Brady L, Nelson PS. RISING STARS: heterogeneity and the tumor microenvironment in neuroendocrine prostate cancer. J Endocrinol. 2023. https://doi.org/10.1530/JOE-22-0211.
11. Merkens L, et al. Aggressive variants of prostate cancer: underlying mechanisms of neuroendocrine transdifferentiation. J Exp Clin Cancer Res. 2022;41(1):46.
12. Yamada Y, Beltran H. Clinical and biological features of neuroendocrine prostate cancer. Curr Oncol Rep. 2021;23(2):15.
13. Ajkunic A, et al. Assessment of TROP2, CEACAM5 and DLL3 in metastatic prostate cancer: expression landscape and molecular correlates. NPJ Precis Oncol. 2024;8(1):104.
14. Lee JK, et al. Systemic surfaceome profiling identifies target antigens for immune-based therapy in subtypes of advanced prostate cancer. Proc Natl Acad Sci U S A. 2018;115(19):E4473-e4482.
15. DeLucia DC, et al. Regulation of CEACAM5 and therapeutic efficacy of an anti-CEACAM5-SN38 antibody-drug conjugate in neuroendocrine prostate cancer. Clin Cancer Res. 2021;27(3):759–74.
16. Bakht MK, et al. Neuroendocrine differentiation of prostate cancer leads to PSMA suppression. Endocr Relat Cancer. 2018;26(2):131–46.

17. Imberti C, et al. CEACAM5-targeted immuno-PET in androgen receptor-negative prostate cancer. J Nucl Med. 2024;65(7):1043–50.
18. Xiao Y, et al. Identification of a CEACAM5 targeted nanobody for positron emission tomography imaging and near-infrared fluorescence imaging of colorectal cancer. Eur J Nucl Med Mol Imaging. 2023;50(8):2305–18.
19. de Gooyer JM, et al. Multimodal CEA-targeted fluorescence and radioguided cytoreductive surgery for peritoneal metastases of colorectal origin. Nat Commun. 2022;13(1):2621.
20. de Gooyer JM, et al. Multimodal CEA-targeted image-guided colorectal cancer surgery using (111)In-labeled SGM-101. Clin Cancer Res. 2020;26(22):5934–42.
21. Zhu XY, et al. A novel human single-domain antibody-drug conjugate targeting CEACAM5 exhibits potent in vitro and in vivo antitumor activity. Acta Pharmacol Sin. 2024;45(3):609–18.
22. Gazzah A, et al. Safety, pharmacokinetics, and antitumor activity of the anti-CEACAM5-DM4 antibody-drug conjugate tusamitamab ravtansine (SAR408701) in patients with advanced solid tumors: first-in-human dose-escalation study. Ann Oncol. 2022;33(4):416–25.
23. Baek DS, et al. A highly-specific fully-human antibody and CAR-T cells targeting CD66e/CEACAM5 are cytotoxic for CD66e-expressing cancer cells in vitro and in vivo. Cancer Lett. 2022;525:97–107.
24. Beauchemin N, Arabzadeh A. Carcinoembryonic antigen-related cell adhesion molecules (CEACAMs) in cancer progression and metastasis. Cancer Metastasis Rev. 2013;32(3–4):643–71.
25. Dotan E, et al. Phase I/II trial of labetuzumab govitecan (Anti-CEACAM5/SN-38 Antibody-Drug Conjugate) in patients with refractory or relapsing metastatic colorectal cancer. J Clin Oncol. 2017;35(29):3338–46.
26. Decary S, et al. Preclinical activity of SAR408701: a novel anti-CEACAM5-maytansinoid antibody-drug conjugate for the treatment of CEACAM5-positive epithelial tumors. Clin Cancer Res. 2020;26(24):6589–99.
27. De Pauw T, et al. Current status and future expectations of nanobodies in oncology trials. Expert Opin Investig Drugs. 2023;32(8):705–21.
28. Turner KB, et al. Improving the targeting of therapeutics with single-domain antibodies. Expert Opin Drug Deliv. 2016;13(4):561–70.
29. Ma J, et al. CDH17 nanobodies facilitate rapid imaging of gastric cancer and efficient delivery of immunotoxin. Biomater Res. 2022;26(1):64.
30. Ding Y, et al. Cadherin 17 nanobody-mediated near-infrared-II fluorescence imaging-guided surgery and immunotoxin delivery for colorectal cancer. Biomater Res. 2024;28:0041.
31. Labrecque MP, et al. Molecular profiling stratifies diverse phenotypes of treatment-refractory metastatic castration-resistant prostate cancer. J Clin Invest. 2019;129(10):4492–505.
32. Guo X, et al. NIR-II fluorescence imaging-guided colorectal cancer surgery targeting CEACAM5 by a nanobody. EBioMedicine. 2023;89:104476.
33. Su W, et al. The polycomb repressor complex 1 drives double-negative prostate cancer metastasis by coordinating stemness and immune suppression. Cancer Cell. 2019;36(2):139-155.e10.
34. Beltran H, et al. The role of lineage plasticity in prostate cancer therapy resistance. Clin Cancer Res. 2019;25(23):6916–24.
35. Dhillon S. Moxetumomab pasudotox: first global approval. Drugs. 2018;78(16):1763–7.
36. Onda M, Kobayashi K, Pastan I. Depletion of regulatory T cells in tumors with an anti-CD25 immunotoxin induces CD8 T cell-mediated systemic antitumor immunity. Proc Natl Acad Sci U S A. 2019;116(10):4575–82.
37. Zhang F, et al. Treatment strategies with combined agency against severe viral pneumonia in patients with advanced cancer. J Transl Int Med. 2024;12(3):317–20.
38. James ND, et al. Docetaxel for nonmetastatic prostate cancer: long-term survival outcomes in the STAMPEDE randomized controlled trial. JNCI Cancer Spectr. 2022;6(4):pkac043.
39. Mahal BA, et al. Mortality risk for docetaxel-treated, high-grade prostate cancer with low PSA levels: a meta-analysis. JAMA Netw Open. 2023;6(11):e2340787.
40. Li S, Kang Y, Zeng Y. Targeting tumor and bone microenvironment: novel therapeutic opportunities for castration-resistant prostate cancer patients with bone metastasis. Biochim Biophys Acta Rev Cancer. 2024;1879(1):189033.
41. Beltran H, et al. Aggressive variants of castration-resistant prostate cancer. Clin Cancer Res. 2014;20(11):2846–50.
42. Tan N, et al. Histological transformation in lung adenocarcinoma: Insights of mechanisms and therapeutic windows. J Transl Int Med. 2024;12(5):452–65.
43. Bakht MK, Beltran H. Biological determinants of PSMA expression, regulation and heterogeneity in prostate cancer. Nat Rev Urol. 2025;22(1):26–45.
44. Hoshi S, et al. PSMA targeted molecular imaging and radioligand therapy for prostate cancer: optimal patient and treatment issues. Curr Oncol. 2023;30(8):7286–302.
45. Davies A, et al. An androgen receptor switch underlies lineage infidelity in treatment-resistant prostate cancer. Nat Cell Biol. 2021;23(9):1023–34.
46. Yao J, et al. DLL3 as an emerging target for the treatment of neuroendocrine neoplasms. Oncologist. 2022;27(11):940–51.
47. Ranallo N, et al. Delta-like ligand 3 (DLL3): an attractive actionable target in tumors with neuroendocrine origin. Expert Rev Anticancer Ther. 2022;22(6):597–603.
48. Alexander E, Leong KW. Discovery of nanobodies: a comprehensive review of their applications and potential over the past five years. J Nanobiotechnology. 2024;22(1):661.
49. Jin BK, et al. NANOBODIES®: a review of diagnostic and therapeutic applications. Int J Mol Sci. 2023;24(6):5994.
50. Boutin L, et al. Camelid-derived Tcell engagers harnessing human γδ T cells as promising antitumor immunotherapeutic agents. Eur J Immunol. 2024;54(8):e2350773.
51. Kreitman RJ, Pastan I. Immunotoxins: from design to clinical application. Biomolecules. 2021;11(11):1696.
52. Shancer Z, et al. Anti-BCMA immunotoxins produce durable complete remissions in two mouse myeloma models. Proc Natl Acad Sci U S A. 2019;116(10):4592–8.
53. Masilamani AP, et al. An anti-PSMA immunotoxin reduces Mcl-1 and Bcl2A1 and specifically induces in combination with the BAD-Like BH3 mimetic ABT-737 apoptosis in prostate cancer cells. Cancers (Basel). 2020;12(6):1648.
54. Leshem Y, et al. SS1P immunotoxin induces markers of immunogenic cell death and enhances the effect of the CTLA-4 blockade in AE17M mouse mesothelioma tumors. Toxins (Basel). 2018;10(11):470.
55. Andersson Y, et al. Immune stimulatory effect of anti-EpCAM immunotoxin - improved overall survival of metastatic colorectal cancer patients. Acta Oncol. 2020;59(4):404–9.
56. Jiang Q, et al. Enhanced efficacy of mesothelin-targeted immunotoxin LMB-100 and anti-PD-1 antibody in patients with mesothelioma and mouse tumor models. Sci Transl Med. 2020;12(550):eaaz7252.

Publisher's Note